

HAWEZ, H.K., SANAE, R. and FAISAL, N.H. 2021. A critical review on coupled geomechanics and fluid flow in naturally fractured reservoirs. *Journal of natural gas science and engineering* [online], 95, article 104150. Available from: <https://doi.org/10.1016/j.jngse.2021.104150>

A critical review on coupled geomechanics and fluid flow in naturally fractured reservoirs.

HAWEZ, H.K., SANAE, R. and FAISAL, N.H.

2021

A critical review on coupled geomechanics and fluid flow in naturally fractured reservoirs

Haval Kukha Hawez¹, Reza Sanaee, Nadimul Haque Faisal

School of Engineering, Robert Gordon University, Garthdee Road, Aberdeen, AB10 7GJ, UK

Abstract

Naturally fractured reservoirs have been a source of challenging issues with regard to field development, well stability, drilling, and enhanced oil recovery, as a connected fracture system can totally dominate the flow patterns. Because of the high degree of heterogeneity in flow characteristics and reservoir geomechanics, several mathematical, numerical and discretization methods are proposed to predict the hydrodynamics behaviour of naturally fractured reservoirs. This paper presents a critical review of the characteristics of naturally fractured reservoirs in terms of geomechanics and fluid flow. In the case of poorly connected fractures and high-density fractured networks, compared to the characteristic length of interest, multi-continuum approaches are widely applicable. The dual continuum approach can handle fracture matrix interaction implicitly much more conveniently than the Discrete Fracture Network (DFN) and Discrete Fracture Matrix (DFM) approaches, but it cannot capture the fracture geometry explicitly where the fracture is the main flow path in the area of interest. Distinct mathematical and numerical modelling of flow and reservoir geomechanics are also addressed in this review paper. In this context, various coupling schemes of reservoir geomechanics and fluid flow are discussed. Recent research challenges related to numerical

23 modelling of multiphase flow, reservoir geomechanics, coupling schemes, and
24 discretisation are also reviewed. It is concluded that despite several research
25 efforts, coupled geomechanics and multiphase flow is still a challenging issue
26 related to mathematical, numerical models and discretisation schemes to capture
27 the hydrodynamic behaviour, such as fracture deformation and fluid flow
28 behaviour, at fracture matrix interaction in naturally fractured reservoirs and
29 adopting the best modelling approach is very much dependent on the desired
30 hydro-mechanical aspects to be investigated.

31 **Keywords:** *Geomechanics, fractured reservoirs, coupling scheme, modelling,*
32 *fracture-matrix interaction.*

33 1.0 Introduction

34 Rigorous numerical modelling of fluid flow in geologically complex reservoirs is a
35 major challenging issue for petroleum reservoir engineers. Conventional and
36 unconventional fractured reservoirs are part of these challenges. Predominantly,
37 fracture network patterns are the main conduits for fluid flow and improve the
38 permeability in tight formations, while the matrix controls the main reservoir
39 storage capacity. Building a modelling framework is a challenging task to describe
40 and understand how single phase and multiphase flow occurs in the fractured
41 reservoirs, and to qualify the hydrodynamic interactions between fractures and
42 adjacent porous matrix under variety of overburden stress levels.

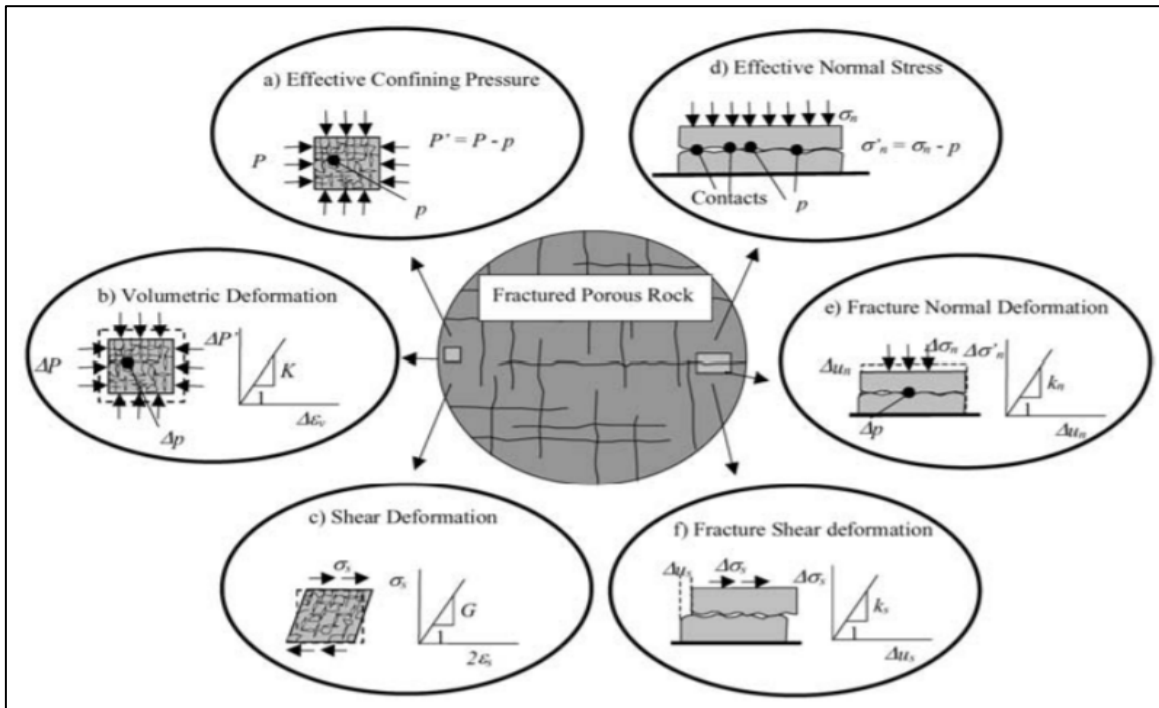
43 Fractured hydrocarbon reservoirs play a significant role both in the world economy
44 and main energy markets. As a result of high heterogeneity and fabric complexity
45 in naturally fractured reservoirs, accurate hydrocarbon recovery predications is

46 challenging despite the existence of giant hydrocarbon reserves in fractured
47 formations (Geiger et al., 2009). Over 20% of the world's reserves and production
48 are provided by natural hydrocarbon reservoirs, such as the Asmari limestone
49 reservoir in Iran, the vugular carbonate reservoirs in Mexico, the Kirkuk oil field in
50 Iraq, the group of chalk reservoirs in the North Sea, and over 400 billion barrels
51 of hydrocarbon reserves in Canada (Abbas, 2000; Jalali and Dusseault, 2012).

52 Fractures are ubiquitous in the subsurface (Berkowitz, 2002) and play a significant
53 role in a wide range of engineering applications, such as nuclear waste disposal,
54 groundwater management, unconventional shale gas reservoirs, geotechnical
55 engineering, and enhanced oil recovery (Abass et al. 2007; Lei, Latham, and Tsang
56 2017; Unsal, Matthäi, and Blunt 2010). The discontinuity of fractures includes
57 complex networks, dominating the geomechanics and hydrogeological behaviour
58 of subsurface rocks (Lei, Latham, and Tsang 2017). The geomechanical analyses
59 play a significant role in demonstrating and characterising phenomena like sand
60 production during the well production, surface subsidence, stability of wells in
61 particular in shale formations, and reservoir compaction where subsurface
62 pressure depletion exists (Jalali and Dusseault, 2012). The main feature of these
63 common phenomena is strongly related to the behaviour of solid interactions with
64 the reservoir fluid flow affected by fractures (Settari and Walters, 2001).

65 The physical interactions of hydraulic and mechanical processes in the porous
66 bearing formation is called hydromechanical coupling (Rutqvist and Stephansson,
67 2003). In petroleum reservoirs, hydromechanical interactions are common due to
68 presence of fractures and pores which are deformable and filled by fluid. In

69 general, porous media or fractured rocks are saturated with fluids, and the porous
 70 media connectivity and fracture apertures can deform as a result of either change
 71 in the external stresses acting on the formation, or change in the internal fluid
 72 pore pressure as shown in Fig.1.



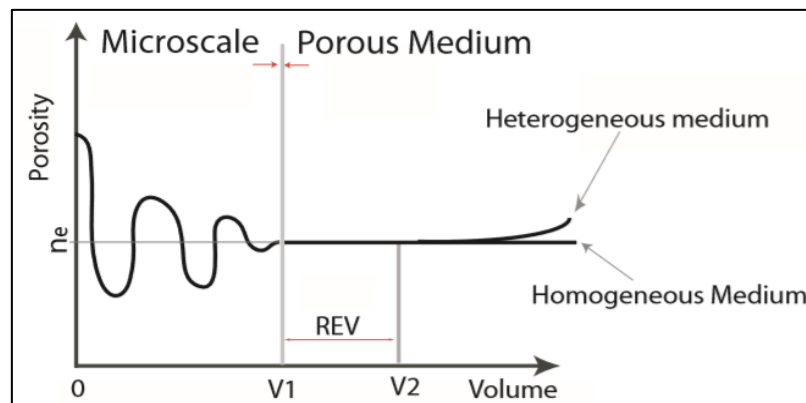
73
 74 *Fig. 1. Overview of the deformation modes in fractured porous media including effects on porous matrix and macro fractures*
 75 *(Rutqvist and Stephansson, 2003).*

76 This paper reviews the most significant fluid flow numerical modelling methods in
 77 fractured porous media. It also provides a comprehensive understanding of
 78 different coupling schemes between reservoir geomechanics and fluid flow in the
 79 fractured porous medium, from physical, conceptual, and mathematical models to
 80 discretization approaches. In addition, it shows the flexibility and complexity of
 81 different flow modelling approaches in fractured porous media, in terms of
 82 computational accuracy and cost. Furthermore, various coupling approaches
 83 related to reservoir geomechanics and fluids are summarised based on the

84 geometrical complexity, flexibility, computational efficiency, and types of
85 discretization.

86 2.0 Modelling of Fluid Flow and Transport in Fractured Porous Media

87 The flow equations in a small volume of porous media (e.g. rock or geological
88 materials), which is representative of elementary volume (REV), was first derived
89 by Bear (1972) (Bear, 1972). Subsequently, mass and momentum conservation
90 equations were used to describe the fluid flow behaviour and transport in fractured
91 porous media. Fig. 2 illustrates the relationship between volumetric porosity and
92 REV, and the fact that porosity measurement changes with sample volume and
93 the domain of the REV (Bear, 1972; Nordahl and Ringrose, 2008).



94

95

Fig. 2. Illustration of the REV concept for porosity (Nick, 2010).

96 In this section, the previous track record of governing flow equations for single
97 and multiphase flow reservoirs are introduced. Furthermore, an extension of
98 Darcy's law in the fractured domain for single-phase flow and physical parameters
99 that govern multiphase flow in fractured reservoirs are highlighted.

100 2.1 Single Phase Flow

101 Darcy transport equation is widely applicable for single, two and three phase flow
102 (Bear, 1972). Eq. (1) represents the Darcy transport equation where the pressure
103 gradient is the major driving force (∇P) for single-phase.

104
$$v = -\frac{k}{\mu} (\nabla P - \rho g \nabla D) \dots\dots\dots (1)$$

105 The mass conservation equation is normally provided by Eq. (2) for single phase
106 flow in the fractured porous media.

107
$$\frac{\partial}{\partial t}(\rho\varphi) + \nabla \cdot (\rho v) = q \dots\dots\dots (2)$$

108 Where: v is the Darcy velocity, ρ is the density of the fluid, μ is the viscosity of the
109 fluid, k is the permeability of the formation, g is the gravitational acceleration, D
110 is the depth of the datum, φ is the rock porosity, and q is the source term.

111 As a result of high flow velocity in the fracture (free channel) domain relative to
112 the porous matrix, Sanaee et al. (2012, 2013) employed the Navier-Stokes
113 equation in fracture volume. In addition, the Brinkman equation, which is an
114 extension of Darcy law (Bars and Worster, 2006), was used to control single phase
115 flow at fracture matrix interactions.

116 2.2 Multiphase Flow

117 In the multiphase flow and isothermal condition, multi-mass components and
118 mass balance equations are needed to describe the flow in fracture and matrix

119 reservoir rocks separately for each phase. Mass conservation equation is given by
120 Eq. (3).

121
$$\frac{\partial}{\partial t}(\varphi S_{\beta} \rho_{\beta}) = -\nabla \cdot (\rho_{\beta} v_{\beta}) + q_{\beta} \dots\dots\dots (3)$$

122 In Eq. (3): $S_{\beta}, \rho_{\beta}, v_{\beta}$ is the saturation, density and velocity for the phase of flow
123 respectively ($\beta = g$ for gas, $\beta = w$ for water, and $\beta = o$ for oil).

124 Darcy law is also widely applied for considering the effect of density, viscosity and
125 pressure gradient for multiphase flow in the fractured porous media as shown in
126 Eq. (4).

127
$$v_{\beta} = -\frac{k_a k_{r\beta}}{\mu_{\beta}} (\nabla P_{\beta} - \rho_{\beta} g \nabla D) \dots\dots\dots (4)$$

128 In Eq. (4): v_{β} is the Darcy velocity of the phase β , μ_{β} is the viscosity of the phase, k_a
129 is the absolute permeability of the formation, $k_{r\beta}$ is the relative permeability of the
130 phase, and ∇P_{β} is the pressure gradient of the phase β .

131 Multiphase (two and three phases) flow modelling is still a challenging task while
132 the most widely used approach is the same one used for single phase flow. To
133 describe multiphase flow in fractured porous media, some more physics should be
134 introduced before proceeding, such as saturations, relative permeability, and
135 capillary pressure (Karimi-Fard and Firoozabadi, 2001; Monteagudo and
136 Firoozabadi, 2004). In the presence of multiphase flow, fluids jointly fill the porous
137 medium indicates the relation (Eq.5) (Zhangxin et al., 2006).

138
$$\sum S_{\beta} - 1 = 0 \dots\dots\dots (5)$$

139 When multi-immiscible fluids exist in the porous media, the distinct pressure
 140 between the non-wetting and wetting phases is called capillary pressure (Eq. 6);
 141 across the interface, pressure arises from the capillary forces and these capillary
 142 forces come from the surface and interfacial tension (Pyrak-Nolte et al., 2008;
 143 Soares et al., 2015).

144
$$(P_c) = P_n - P_w \dots\dots\dots (6)$$

145 where: P_c stands for capillary pressure, P_n and P_w are the non-wetting and wetting
 146 phases' pressures respectively.

147 In immiscible multiphase flow, the presence of the non-wetting phase decreases
 148 the cross-sectional area availability to flow of wetting fluid and vice versa.
 149 Therefore, the ability of fluid to transport reduces within porous media domain
 150 and is defined by relative permeability (Falode and Manuel, 2014; Honarpour et
 151 al., 1986; Jerauld and Salter, 1990).

152
$$k_{r\beta} = \frac{k_{\beta}}{k_a} \dots\dots\dots (7)$$

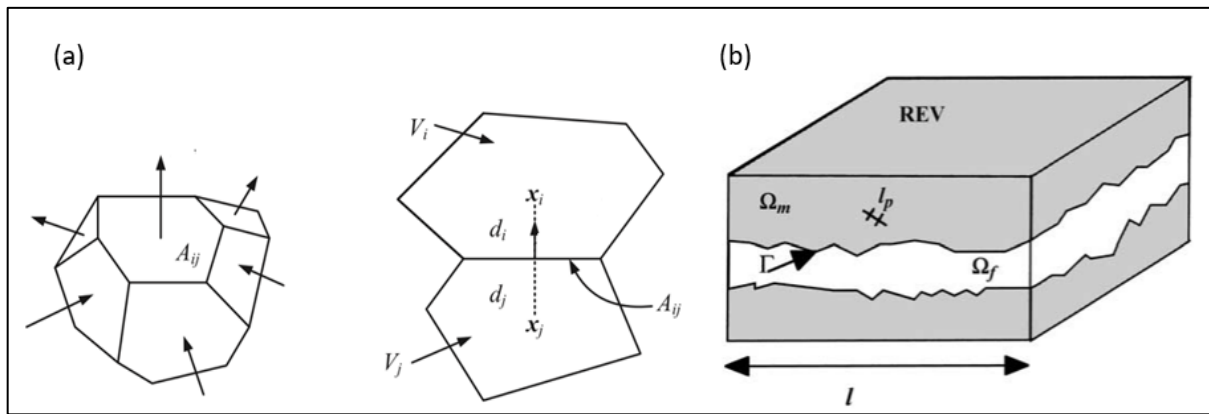
153
$$\lambda_{\beta} = \frac{k_{r\beta}k_a}{\mu_{\beta}} \dots\dots\dots (8)$$

154 where: k_{β} is the effect permeability of the phase, k_a is the absolute permeability
 155 and λ_{β} is the mobility of the phase.

156 Adding Eqs. (7) and (8) to Eq. (2), then Eq. (9) describes multiphase
 157 incompressible fluid flow in the porous media.

158
$$\frac{\partial}{\partial t} (\varphi S_{\beta} \rho_{\beta}) = \nabla \cdot (\rho_{\beta} \lambda_{\beta} (\nabla P_{\beta} - \rho_{\beta} g \nabla D)) + q_{\beta} \dots\dots\dots (9)$$

159 However, flow behaviour cannot be investigated alone by Eq. (9) in different
 160 continuums. Therefore, it is essential to specify the initial and boundary conditions,
 161 and the continuity equation must be detected at different interfaces between
 162 distinct continua in terms of pressures, concentrations and mass fluxes (Martin et
 163 al., 2017). Fig. 3(a) represents the flow term evaluation, spatial discretization and
 164 grid block connections within a multi-continuum system between two neighbour
 165 grid blocks (i, j) directly based on the integrated finite difference approach. Fig.
 166 3(b) illustrates the effect of the periodic domain system (Ω) which is the effect of
 167 fracture length on the contaminant transport in the fractured porous media at the
 168 macroscopic scale where multiple fracture scales exist (Kalinina et al. 2014; Wu
 169 et al. 2006).



170
 171 Fig. 3. (a) 2D Finite difference integration for flow term evaluation, spatial discretization and connection (Wu 2016). (b)
 172 Fractured porous media domain, REV (Representative Elementary Volume), Ω_f (fracture domain), Ω_m (matrix domain), Ω
 173 (Periodic domain), l (microscopic characteristics length), l_p (the pore lengthscale), Γ (fracture-matrix boundary or interface)
 174 (Royer et al., 2002).

175
 176 3.0 Conceptual Flow Modelling of Fractured Rocks

177 A conceptual model describes the main geological and hydrogeological features of
 178 the fractured porous media that control the transport and fluid flow behaviour in

179 the system (Berkowitz, 2002). The realistic development of conceptual models for
180 multiphase flow in fractured rocks is a significant research problem for enhanced
181 oil recovery, nuclear waste disposal, and subsurface contamination (Council,
182 1996).

183 In the past few decades, several mathematical modelling approaches have been
184 developed and extended. They mainly depend on continuum approaches involving
185 geometrical information for fracture and matrix formation systems, setting up the
186 domain of the fracture matrix system for mass and energy conservation equations
187 (Lei, Liao, and Zhang 2019; Wu, Liu, and Bodvarsson 2004). These approaches
188 are followed by solving discrete nonlinear algebraic equations numerically which
189 couple fluid flow phases with other physical processes (Warren and Root 1963;
190 Wu 2016).

191 3.1 Single Continuum Approach

192 The single continuum approach states that both fracture and matrix are in the
193 same domain, and fractured permeability is adapted by the porous matrix domain.
194 The fluctuation of permeability tensor and its orientation might vary, based on the
195 fracture properties and network. The volume average of this approach is ideally
196 expressed by representative elementary volume (REV) (Bear, 1972; Berre et al.,
197 2019).

198 In the single continuum method, transport is transfigured from a microscopic to a
199 macroscopic scale when the average of microscopic quantities are used for the

200 problem (Dadzie et al., 2008). The whole domain's exact local characteristics are
201 covered by the use of average quantities of REV.

202 The heterogeneity size is much smaller than the size of REV and the size of the
203 REV must be smaller than the microscopic length scale. This method allows REV
204 to be determined, and then the continuum approach is applicable in a fractured
205 reservoir. The physical behaviour upscaling method of the macroscopic level can
206 be derived by the REV scale. In general, Darcy's law is applied for flow in the single
207 continuum approach where the flow is essentially influenced by frictional
208 resistance and the pressure gradient is the major driving force in the system as
209 already discussed (Royer et al., 2002).

210 3.2 Dual Continuum Approach

211 The dual continuum approach represents the fracture and matrix domains
212 separately, such as with dual porosity and dual permeability values. The dual
213 continuum approach can involve several fractures or fracture networks locally and
214 is expressed by representative elementary volume (REV) (Wu 2016).

215 The dual continuum method has been advanced and used as the main method for
216 modelling fluid flow, heat transfer, and chemical transportation in fractured porous
217 media (Wu, Pan, and Pruess 2004). Furthermore, the physical process of fluid flow
218 and transport in fractured reservoir rocks are treated separately for each
219 continuum, such as fracture continuum and matrix continuum. The same basic
220 conservation of mass, energy and momentum are governed for flow within each
221 continuum separately (Khalili 2008; Wu and Qin 2009). Although, it should be

222 noted that the dual continuum approach depends on the uniform distribution of
223 denser fracture networks, and detailed information of fracture and matrix
224 characteristics. The dual continuum approach is widely used in petroleum reservoir
225 simulation and in commercial reservoir simulators (Moinfar et al., 2011;
226 Monteagudo and Firoozabadi, 2004).

227 Multiphase flow is described separately, in naturally fractured formations, for both
228 continua matrix and fracture using doublet flow equations in the dual continuum
229 approach. This method causes a set of partial differential equations for both
230 continua (Wu, Pan, and Pruess 2004).

231 3.3 Triple Continuum Approach

232 The triple continuum approach is developed in the same way as Warren and Root's,
233 used for the dual-porosity model; both matrix systems are considered locally
234 uniform and homogenous. There may exist an important heterogeneity within the
235 rock matrix and fractures systems. The concept of double porosity has been
236 extended to explore the effect of heterogeneity on flow in fractured and rock
237 matrix (Wu, Pan, and Pruess 2004). In addition, a number of triple continuum
238 methods have been progressed and used to carry out the effect of rock matrix
239 heterogeneity, small fractures, and for vuggy fractured reservoirs. In general,
240 these multi-continuum approaches have concentrated on distinct levels and scales
241 of the lithological heterogeneity of fractures and rock matrix. This includes
242 subdividing the fractures and matrix systems through two or more subdomains
243 with distinct characterizations for single and multiphase flow in fractured porous
244 media (Wu 2016).

245 Furthermore, the fracture–matrix system is conceptualized as a triple continuum
246 model to explore the effects of small-scale fractures in fractured reservoirs. This
247 includes single porous rock matrix and two kinds of fractures: (1) large fractures
248 which globally connect to other fractures; and (2) small fractures that are locally
249 connected to the large fractures and the rock matrix (Wu, Pan, and Pruess 2004).

250 In principle, the triple continuum approach is similar to a dual continuum approach
251 for small fractures. The entire reservoir volume is occupied by three distinct spatial
252 continua (vug, fracture and matrix) that use effective porosity values to
253 approximate the two fracture types (small and large) and rock matrix (Wu 2016).

254 3.4 Discrete Fracture Network Model (DFN)

255 In general, the DFN concept is a comprehensive study of fractured rock modelling
256 and it is a group of geometrical planes that represent fractures (Tavakkoli et al.,
257 2009). In DFN modelling, the model domain of the formation includes every
258 fracture pattern’s properties (e.g. orientation, size, position, shape and aperture)
259 and flow description, explicitly through fractured systems at fracture matrix
260 interaction. A discrete fracture model is a rigorous approach for the field scale as
261 opposed to other fracture modelling approaches because of computational
262 intensity and large data requirement (Lei, Latham, and Tsang 2017).

263 In addition, the number of fractures involved in the field simulation is vast, and
264 this approach usually requires the detailed characteristics of fracture and matrix
265 properties and their spatial distributions – which are hardly familiar from the field
266 site in fractured reservoirs. The DFN model commonly disregards the host domain

267 and ignores the flow in the matrix domain, and considers the impenetrability of
268 the matrix domain (Lei, Latham, and Tsang 2017). In the DFN model, it is assumed
269 that only a fracture network can contain and store fluid which is represented by
270 lattice. A DFN model is commonly used and appropriate where (1) the porous
271 media is explicitly presented by entire porosity and permeability of the fracture;
272 and (2) the network represents a model of fractures in low permeable porous
273 media (Berre, Doster, and Keilegavlen 2019; Wu 2016).

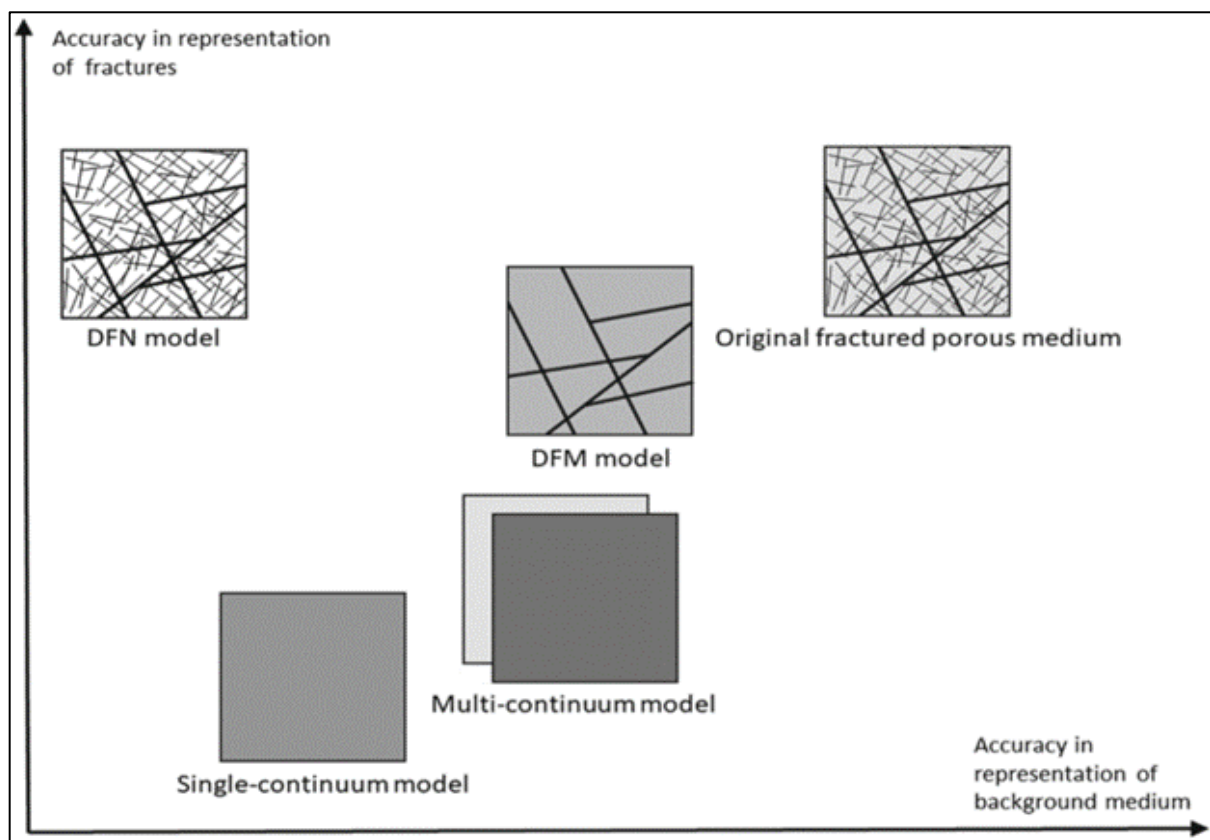
274 3.5 Discrete Fracture-Matrix Model (DFM)

275 The discrete fracture-matrix model was first introduced by (Noorishad and Mehran,
276 1982), commonly referred to as the DFM model. The main concept of the discrete
277 fracture-matrix model is based on the equilibrium cross flow between the fluids in
278 the fracture node to the rock matrix node next to the fracture (Monteagudo and
279 Firoozabadi, 2004). The DFM model attempts to create a balance between loss of
280 accuracy and applying geometric complexity by upscaling. Fluid flow is explicitly
281 represented in the fracture and matrix domain, and this model allows the creation
282 of a length of fracture, much less than the size of the matrix domain. Therefore,
283 the DFM model provides secondary permeability in the fracture domain, rather
284 than being part of the explicit fracture network, as in the DFN model (Berre et al.,
285 2019).

286 Although all the fractures can be incorporated in the fracture domain and within
287 the governing equations, it is not practicable to retain an explicit representation
288 of all fractures because of the computational complexity. Therefore, some of the

289 fractures are preserved, while others are upscaled and replaced by averaged
290 quantities within the matrix domain (Keilegavlen et al., 2017).

291 The DFM model can be used in the detailed modelling of the interface of two phase
292 flow, capillary pressure and hydromechanical interaction between flow and the
293 matrix medium even if the matrix medium is considered as impermeable (Berre
294 et al., 2019). Fig. 4 highlights a generalized picture of different conceptual models
295 for fractured medium, and how the different conceptual models might relate to
296 examine the specific problem in the fractured porous media. The application of
297 different conceptual models in comparison to others is based on the existence of
298 the separate scales fractured medium, along with the availability of the original
299 information.



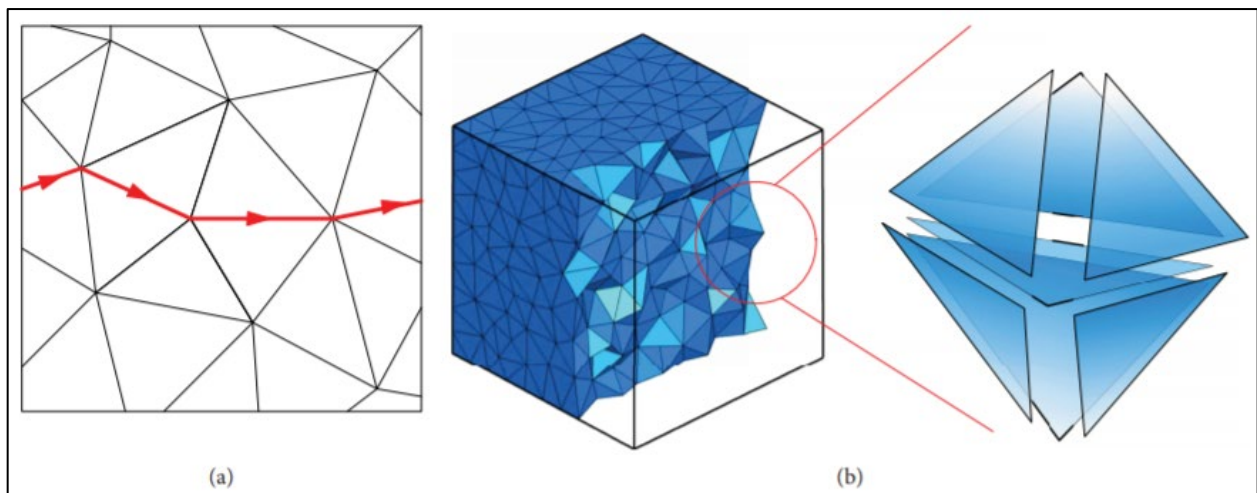
300
301

Fig. 4. Illustrating the fractured porous media model concepts (Berre et al., 2019).

302 4.0 Numerical Flow Modelling of Fractured Rocks

303 The fractured fluid flow and transport behaviour of the system is normally
304 estimated by numerical models, described by conceptual models such as two and
305 three dimensional (2D, 3D) equivalent fracture matrix networks (Yao et al., 2019).
306 Fig. 5(a) illustrates a simplified 2D representation of the solid red streamline,
307 where the triangular interfaces are diminished to the line segments in the model.
308 A 3D schematic concept of the network interface is also depicted in Fig. 5(b),
309 where the main fluid paths are between tetrahedrons in the triangular interfaces.
310 Flow geometry provides the mathematical formulations of the numerical models
311 specified in the conceptual model (Council, 1996).

312 In general, several numerical methods have been developed and progressed based
313 on the conceptual models for fluid flow modelling, based on their classification for
314 the complexity and treatment compatibility in fractured porous media (Blunt,
315 2001; Unsal et al., 2010; Yao et al., 2019; Zhang et al., 2019).



316

317

Fig. 5. Conceptual representation fluid flow in equivalent fracture and matrix models in 2D and 3D (Yao et al., 2019).

318 *4.1 Numerical Modelling of Single Continuum Approach*

319 The single continuum approach treats the fractured rock system as a continuous
320 body that can be determined implicitly by the old finite difference method and
321 finite element method. In addition, this is the simplest method and gives the single
322 value of porosity and permeability for the fractured domain. The proper application
323 case of the single continuum approach is when a single continuous fracture in the
324 domain is being modelled (Berre, Doster, and Keilegavlen 2019; Jing 2003; Lei,
325 Latham, and Tsang 2017).

326 *4.2 Numerical Modelling of Dual Continuum Approach*

327 In the dual continuum implicit approach, finite element method and finite volume
328 or difference discretization schemes are typically used for discretization of the fluid
329 flow process in fractured porous rocks. It is a practical approach to investigate and
330 understand the behaviour of coupled mechanics of multiscale systems (Ashworth
331 and Doster, 2019; Monteagudo and Firoozabadi, 2004). However, these models
332 are limited to sugar cubic representations of a fractured system. Another limitation
333 is the fluid flow exchange term between the fractured domain and matrix, and the
334 exchange term may not be suitably defined by gravity and viscous effects only
335 (Monteagudo and Firoozabadi, 2004).

336 Furthermore, there is a huge number of advancements of control volume methods
337 for flow discretization such as two-point flux approximations (TPFA), nonlinear
338 two-point flux approximation methods (NTPFA), Multipoint flux approximations
339 (MPFA), mixed finite element (MFE), and mimetic finite difference (MFD) (Arrarás,
340 Portero, and Jorge 2010; Berndt et al. 2001; Karimi-Fard and Durlofsky 2016;

341 Klausen and Russell 2004; Lipnikov, Manzini, and Svyatskiy 2011; Wang et al.
342 2016; Zhang and Abushaikha 2019).

343 The two-point flux approximation (TPFA) is the straightforward method for
344 discretization where the flux is approximated by using the pressure in the two
345 grids sharing the edge. However, TPFA does not provide a dependable flux, is not
346 convergent, and is not suitable to resolve the flow field accurately. But, it is easy
347 to formulate, employ, and does not suffer from artificial oscillations (Droniou,
348 2014).

349 To employ large grid stencils and considering the transmissibilities as a function
350 of the solution of the fluxes, significant progress has been done for the traditional
351 TPFA which involves the computational complexity denoted to nonlinear two-point
352 flux approximation (NTPFA) (Chen et al., 2008).

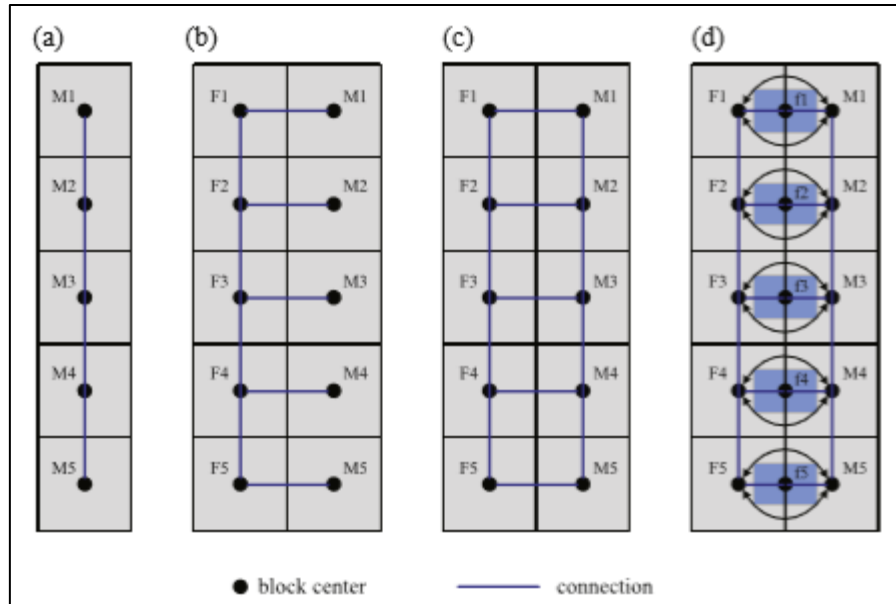
353 It is worth mentioning that the flux over an edge cannot be approximated properly
354 by using a linear amalgamation in the two adjacent cells. Therefore, the multipoint
355 flux approximation (MPFA) has been progressed independently by (Aavatsmark et
356 al., 1996) to involve the non-linear approximation, adjust the flux expression, and
357 to consist of more points in the flux stencil (Aavatsmark et al., 2010, 2008, 1998).
358 Furthermore, several local conservative methods have been developed to control
359 volume methods and discontinuity of the permeability tensors such as mixed finite
360 elements (MFE) and mimetic finite differences (MFD) (Klausen and Russell, 2004).

361 In addition, many of the computational efforts are started solving nonlinear and
362 thereby linear systems in the field of applications. The main significant factor for

363 fast solvers of MPFA is to achieve popularity and to formulate a suitable
364 mathematical framework for the analysis of the methods (Droniou, 2014). The
365 analysis of convergence is still based on the relations between MPFA methods and
366 MFE or MFD discretization (Wheeler and Yotov, 2006).

367 *4.3 Numerical Modelling of Triple Continuum Approach*

368 The main purpose of using this approach is when the vuggy, fractured porous
369 matrix, or two different scales of fractures and rock matrix are available. The triple
370 continuum approach treats the vuggy fracture matrix system separately, as three
371 distinct continua. The finite element methods are used implicitly for modelling of
372 fluid flow, aided with the controlled volume or finite difference method (Wu 2016;
373 Youssef and Alnuaim 2017). The comparisons of the triple continuum approach
374 with the single continuum and dual continuum (dual porosity and dual
375 permeability) approaches are depicted in Fig. 6. In general, the concept of the
376 triple continuum approach is an extension of the dual continuum approach by
377 computing one more network of small fracture between large fractures and matrix
378 blocks as shown in Fig. 6(d).



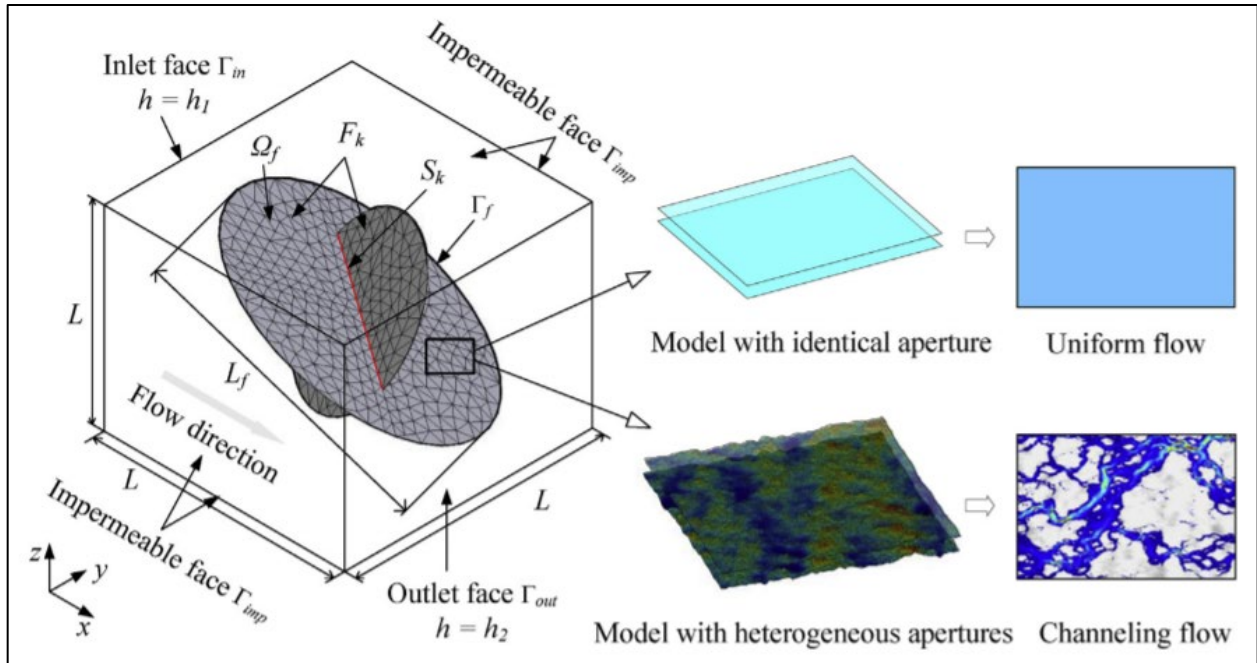
379

380 *Fig. 6. Illustrating distinct conceptualization for fracture matrix treatment (a) Single Effective Continuum Approach (b) Dual*
 381 *Porosity Approach (c) Dual Permeability Approach (d) Triple Continuum Approach (F=large fracture, f=small fractures, and*
 382 *M=matrix) (Wu 2016; Wu, Liu, and Bodvarsson 2004).*

383

384 4.4 Numerical Modelling of Discrete Fracture Network Model (DFN)

385 A discrete fracture network (DFN) is based on the premise that the subsurface
 386 flow and transport occur mainly within the fractures, and there is no space
 387 between the fractures except the location of their intersection. Therefore, the
 388 concept of DFN is used to interpret the fracture and fracture set properties. The
 389 DFN represents fracture characterization such as orientation, size, spatial
 390 distribution, shape, and transmissivity explicitly (Barton et al., 2013). The 3D
 391 DFNs provide single aperture values per fracture, because the simplifications of
 392 fracture heterogeneity may introduce errors in estimating the hydraulic response
 393 in the fractured rock masses as illustrated in Fig. 7 (Huang et al., 2019).



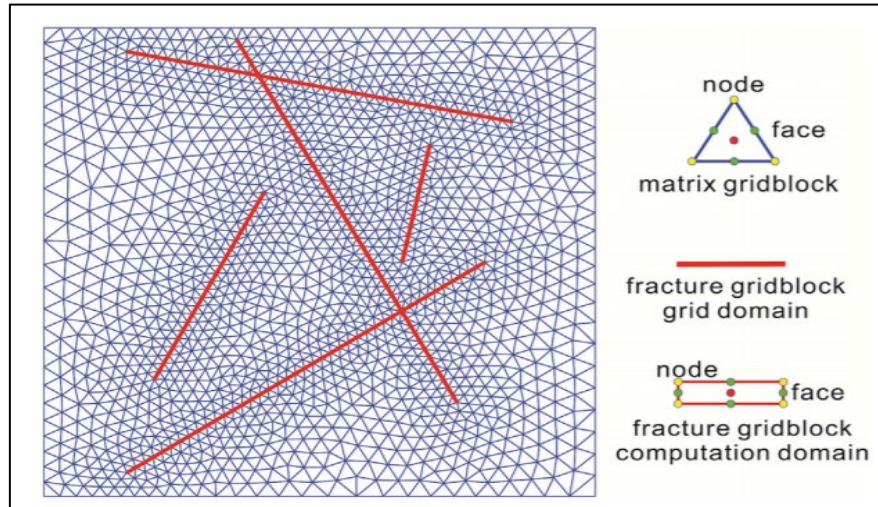
394

395 *Fig. 7. Representation of 3D DFN fracture aperture distributions and different hydraulic response results, where L_f/L is the*
 396 *fracture length to the domain length, h is the hydraulic head, F_k is the set of fracture intersection, Γ_f is the border of the*
 397 *fracture domain Ω_f , and Γ_s is the fracture intersection (Huang et al., 2019).*

398 4.5 Numerical Modelling of Discrete Fracture Matrix Model (DFM)

399 In the last decade, the discrete fracture matrix model has received considerable
 400 attention for simulating naturally fractured reservoirs. Most DFM models focus on
 401 unstructured grids to conform to the geometry and the location of the fractures
 402 (Moinfar et al., 2014). Fig.8 highlights the unstructured mesh which is triangular
 403 based and subdivided into 2D, 1D, and 0D objects. The DFMs can produce the real
 404 geometry of the fracture explicitly and each of the fractures has its own size,
 405 shape, orientation, and permeability (Yang et al., 2020). Therefore, the DFMs
 406 account for the effect of every individual fracture on fluid flow in the fractured
 407 porous medium (Karimi-Fard and Firoozabadi 2003). Endeavours toward the
 408 development of DFMs based on the finite element method by (Baca et al., 1984),
 409 and later (Marcondes and Sepehrnoori, 2010) resulted in the implementation of

410 control volume and finite element methods to simulate fracture and flow in the
411 fractured reservoirs.



412
413

Fig. 8. 2D schematic of DFM (Zhao et al. 2018).

414 Much research effort was given to the study of outcrop characterisation, and
415 illustration of significant changes in fractures' height, aperture, space, length, and
416 network connectivity (Karimi-Fard, Durlofsky, and Aziz 2003; Lee and Schechter
417 2015; Lu Li, Shi, and Wang 2019; Monteagudo and Firoozabadi 2004; Xia Yang et
418 al. 2018). However, there was a large discrepancy in terms of realization and
419 uniformity in dual porosity assumptions. The discrete fracture matrix model has
420 been developed to reduce the number of nonphysical notions in the dual
421 continuum approach. The majority of DFMs focused on the unstructured grids to
422 explicitly represent fractured porous rocks. DFM has several advantages, such as
423 the realistic simulation of the geometry of fractures, and the effect of each
424 individual fracture. It is easy to update fracture models in this approach because
425 they are not constrained with grid-defined geometry of fractures. In contrast, the
426 discrete fracture matrix models requires solving discrete systems of equations and

427 hence a complex structure and more difficulty in solving numerically (Moinfar et
428 al., 2011). In addition, the DFMs will provoke a generous number of refined grids
429 around the position where the fractures intersect or densely distributed, which
430 leads to low computational efficiency (Zhao et al., 2018). Therefore, the DFM
431 approach was further integrated and elaborated to deliver an embedded discrete
432 fracture model (EDFM) (Lee et al., 2001; Li and Lee, 2008). In general, EDFMs
433 have straightforward mathematical algorithms for producing grids and will not
434 produce many refined grids compared to DFMs when the fractures have complex
435 geometric features. A structured mesh is also employed to discretize the matrix
436 system in EDFMs and fractures are embedded into the background mesh to be
437 divided into some fracture grids (Yang et al., 2020). It is also stated that the
438 EDFMs have high computational efficiency as a result of avoiding the struggle in
439 creating and recreating high quality conforming mesh (Rao et al., 2019).
440 Furthermore, different types of fracture network models demonstrate different
441 strengths in various aspects but might all suffer from some drawbacks, as listed
442 in Table 1. Table 1 also provides a detailed comparison of distinct fracture network
443 models.

Table 1: Comparison between various numerical flow modelling of fractured rocks.

Numerical Methods (models)	Input Parameters	Advantages	Limitations
Single continuum approach	Material properties of matrix.	<ul style="list-style-type: none"> Reduces geometrical complexity. Suitable for large scale of application. Uses deterministic or stochastic models. Productive calculation. 	<ul style="list-style-type: none"> No consideration of matrix porous media. No fracture and matrix interaction, displacement and rotation. Implicit generation of system. Valid only for using REV (Council 1996; Lei, Latham, and Tsang 2017). Uniform value of porosity and permeability (Youssef and Alnuaim, 2017).
Dual continuum approach	Properties of fracture and matrix.	<ul style="list-style-type: none"> Simplicity of geometry. Suitable for large scale of application. Two separate continua (matrix and fracture). Uses deterministic or stochastic models. 	<ul style="list-style-type: none"> Implicit generation of system (Ashworth and Doster, 2019). Continuity of the fractures. Valid only for using REV (Council 1996; Lei, Latham, and Tsang 2017). Limited to sugar cube representation of fracture domain. Needs fluid flow exchange term between fracture and rock matrix (Monteagudo and Firoozabadi, 2004).
Triple continuum approach	Material properties of fractures, matrix rocks and vugs.	<ul style="list-style-type: none"> Three separate continua (matrix, fracture and vug or matrix, small fracture and large fracture) (Youssef and Alnuaim, 2017). Suitability of use for large scales. Uses deterministic or stochastic models. 	<ul style="list-style-type: none"> Implicit generation for all systems. Continuity of the fractures. Valid only for using REV (Council 1996; Lei, Latham, and Tsang 2017). Needs fluid flow exchange term between fracture and rock matrix (Monteagudo and Firoozabadi, 2004).
Discrete fracture network model	Material properties of fractures and fracture sets.	<ul style="list-style-type: none"> Includes discontinuous fractures. Explicit generation of the effect of each individual fractures on fluid flow (Monteagudo and Firoozabadi, 2004). 	<ul style="list-style-type: none"> Fracture is the main store of fluid to flow towards the wellbore. Rock matrix is impermeable. Intensive computational time (McClure and Horne, 2013). Can found only by stochastic and probabilistic models.
Discrete fracture matrix model	Material properties of fractures, fracture sets and matrix blocks.	<ul style="list-style-type: none"> Includes discontinuous fractures and matrix blocks. No need for fluid exchange term between fracture and matrix interface. Explicit generation of the effect of each individual fractures on fluid flow (Monteagudo and Firoozabadi, 2004). 	<ul style="list-style-type: none"> Intensive computational time. Conforming unstructured mesh. Losing local mass conservation quality while modelling for multiphase flow (Karimi-Fard, Durlofsky, and Aziz 2004). Can found only by stochastic and probabilistic models. Numerical instability of the flow computation (Fleishmann et al., 1999).
Embedded Discrete Fracture Model	Material properties of fractures, fracture sets and matrix blocks.	<ul style="list-style-type: none"> Includes discontinuous fractures and matrix blocks. Most popular and accurate numerical flow modelling (Dong et al., 2019). Explicit generation of the effect of each individual fractures on fluid flow (Monteagudo and Firoozabadi, 2004). Conforming structured mesh. 	<ul style="list-style-type: none"> Intensive computational time. Losing local mass conservation quality while modelling for multiphase flow (Karimi-Fard, Durlofsky, and Aziz 2004). Numerical instability of the flow computation

1 5.0 Geomechanical Characterization

2 Geomechanical record observations trace back to AD 77, when two men observed
3 that the level of water in a well corresponded to the ocean tides, and they recorded
4 this phenomenon in a book (Zhao 2012). Since then, geomechanical research has
5 progressed consistently. As petroleum exploration and production significantly
6 increased, more physical phenomena related to geomechanics have been observed
7 in the oil and gas reservoirs in the early 20th century. For instance, Goose Creek
8 oil field was reported to sink into the water in 1918 and this subsidence was caused
9 by oil and gas extraction (Pratt and Johnson, 1926). Later, the physical hypothesis
10 was developed by Biots, and other scientists behind various observations in the
11 petroleum industry.

12 5.1 Constitutive Relations

13 The hypothesis of geomechanics, through a series of laboratory experiments, was
14 first presented by Karl Terzaghi (Terzaghi et al., 1996). In these laboratory
15 experiments, a constant load was applied laterally for a saturated soil sample. This
16 hypothesis was depicted by the following equation:

17
$$\frac{\partial p}{\partial t} = c \frac{\partial^2 p}{\partial l^2} \dots\dots\dots (10)$$

18 where p is the pore pressure, t is time, c is the consolidation coefficient and l is
19 the length of the soil sample.

20 The concept and definition of effective stress were then defined by Karl Terzaghi,
21 as he noticed that effective stress, which is the difference between pore pressure

22 and externally applied stresses, controls the behaviour of the saturated soil
23 samples as depicted in Fig. 9 (Zoback, 2007).

24
$$\sigma_{i,j} = \sigma'_{i,j} \pm \delta_{i,j}p \dots\dots\dots (11)$$

25 where $\sigma_{i,j}$ is the total stress, $\sigma'_{i,j}$ is the effective stress, $\delta_{i,j}$ is the Kronecker delta
26 in i and j volume respectively.

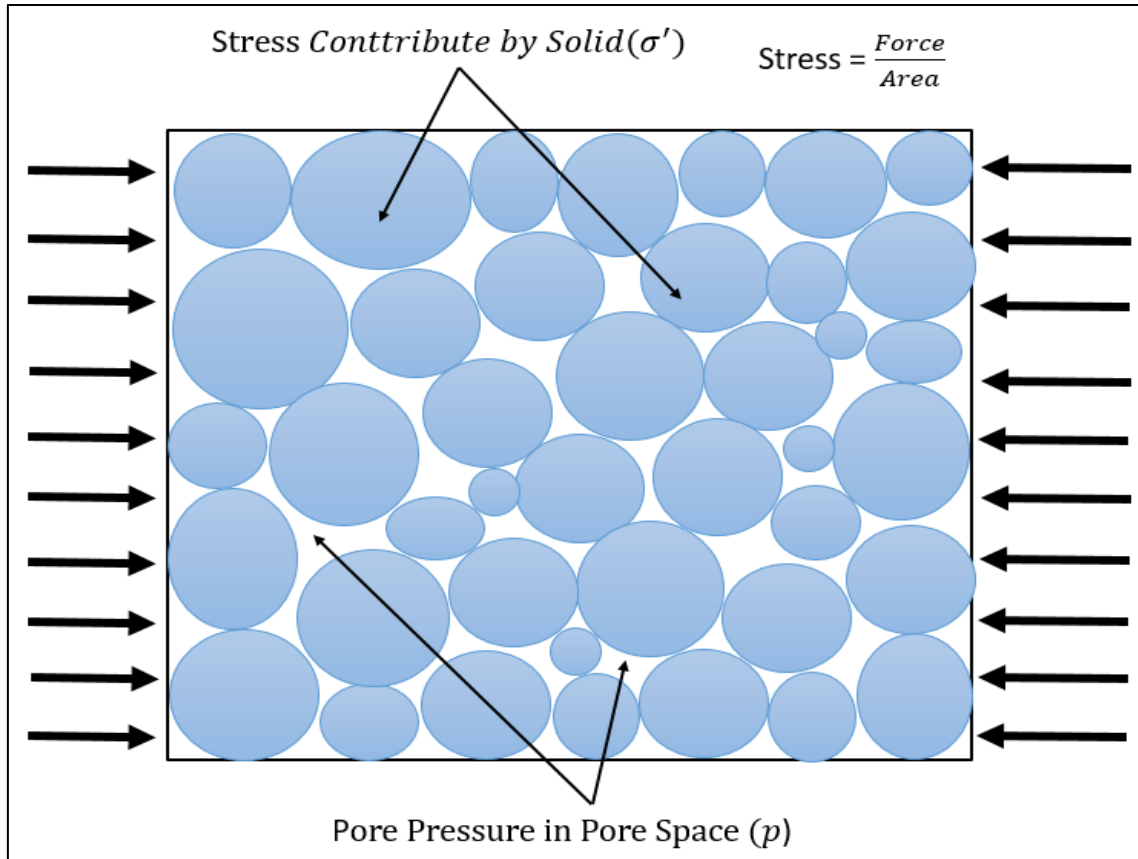
27 The + and - signs depend on the direction of externally applied stresses. If the
28 external stresses are defined as positive, then + should be used (Zhao 2012).
29 Then, the Biot Willis Coefficient (α) parameter is identified as the drained and solid
30 bulk moduli of material (Garg and Nur, 1973; Nur and Simmons, 1969).

31
$$\sigma_{i,j} = \sigma'_{i,j} \pm \alpha \delta_{i,j}p \dots\dots\dots (12)$$

32 Biot Willis coefficient can be calculated as in Eq. 13.

33
$$\alpha = 1 - \frac{K_d}{K_s} \dots\dots\dots (13)$$

34 where K_d is the drained bulk moduli of material and K_s is the solid bulk moduli of
35 material (Biot 1962). The typical value of α is between 0 and 1. For the compacted
36 and nearly solid rocks, the value of α is zero when there are no interconnected
37 pores, and pore pressure has no impact on rock behaviour, such as in quartzite.
38 In contrast, the value of α is equal to one for highly interconnected pores, and
39 indicates pore pressure has a maximum influence such as the case of (uncemented
40 sands) (Zoback, 2007).



41

42

Fig 9. Demonstration of effective stress and pore pressure (Zoback, 2007).

43

A theoretical governing equation system for three dimensional (3D) consolidation was then developed by Biot (1941). The Biot 3D consolidation model is considered as the basis of computational geomechanics which illustrates pore pressure variation with solid consolidation. This model was then further expanded to describe dynamic behaviour in the soil (Biot 1956). Some theories were developed later to model fluid flow in soil consolidation based on the Biot theory (Green and Naghdi, 1970).

50

In summary, the basic constitutive relations mentioned above are used to describe porous material deformation behaviour under different stress loading. The major geomechanical constitutive relations are categorised as the elasticity,

52

53 poroelasticity and thermoporoelasticity models that are widely employed in
54 petroleum reservoir simulation (Zhao 2012). Due to the complexity of the porous
55 material behaviour observations under different stress loading, some
56 simplifications of the geomechanical constitutive relations were made based on
57 natural geomechanical phenomena. The geomechanical constitutive relations are
58 expressed as linear and nonlinear mathematical formulation, based on the
59 requirements of the practical applications (Bemer et al., 2001). The linear
60 poroelasticity model is widely used in fractured porous rocks to investigate the
61 mechanical change due to the pressure depletion in the fractured reservoirs
62 (Bagheri and Settari, 2005; Bai et al., 2019; Garipov et al., 2016; Ren et al.,
63 2018; Sanaee et al., 2013; Sangnimnuan et al., 2018; Yang et al., 2018). Another
64 significant use of geomechanical constitutive relations is to inform when the
65 material reaches plasticity behaviour and eventually collapses. In the reservoir
66 simulation point of view, this phenomenon is significant in recovering oil and gas
67 when the fracture is the main path to flow in the fractured porous rock reservoirs.

68 5.2 Geomechanical Modelling of Fractured Rocks

69 In general, numerical approaches in geomechanical modelling are categorized for
70 both continuum and discontinuum methods based on their taxonomy and
71 treatment displacement compatibility (Jing, 2003; Lei et al., 2017). Continuum
72 and discontinuum numerical approaches have been employed to accelerate
73 computer power and defeat the simplified analytical hypothesis (Manouchehrian
74 et al., 2012). The continuum approach has greater efficiency to handle the
75 enormous problems, while the discontinuum approach can more accurately
76 integrate complicated fracture networks and fragmentation processes. In addition,

77 the discontinuum approaches can handle the continuous deformations, whereas
78 there are some advanced continuum techniques to consider the discontinuities
79 which are included contact algorithms and fracture mechanics (Lei et al., 2017).
80 Several numerical methods and codes have been developed and progressed for
81 geomechanical modelling, based on their classification for the compatibility in
82 handling displacements – in classical mechanical problems with little modifications
83 (Cundall, 1988; Figueiredo et al., 2015; Jing, 2003; Potyondy and Cundall, 2004;
84 Tham et al., 2004). The preference for using a method for geomechanical
85 modelling depends on the scale of the problem and the complexity of the fracture
86 network system. There is a huge number of numerical approaches such as finite
87 element method (FEM), finite difference method (FDM), boundary element method
88 for continuum approaches and discrete element method (DEM), and discontinuous
89 deformation analysis (DDA) for discontinuum approaches (Bobet, 2010).

90 [5.2.1 Continuum Approaches](#)

91 In the conventional continuum approaches, the rock domain is assumed to be
92 continuous and solved by finite difference method (FDM), finite element method
93 (FEM), or boundary element method (BEM) (Bobet, 2010; Pang et al., 2016). The
94 continuum approach is only applicable when a few or a large number of fractures
95 exist (Jing, 2003).

96 The finite difference method (FDM) is based on the discretization of the governing
97 partial differential equations (PDEs) by following partial derivatives with
98 differences described at neighbour grid points (Jing and Hudson, 2002). The set
99 of linear differential equations are employed by FDM which can be solved by any

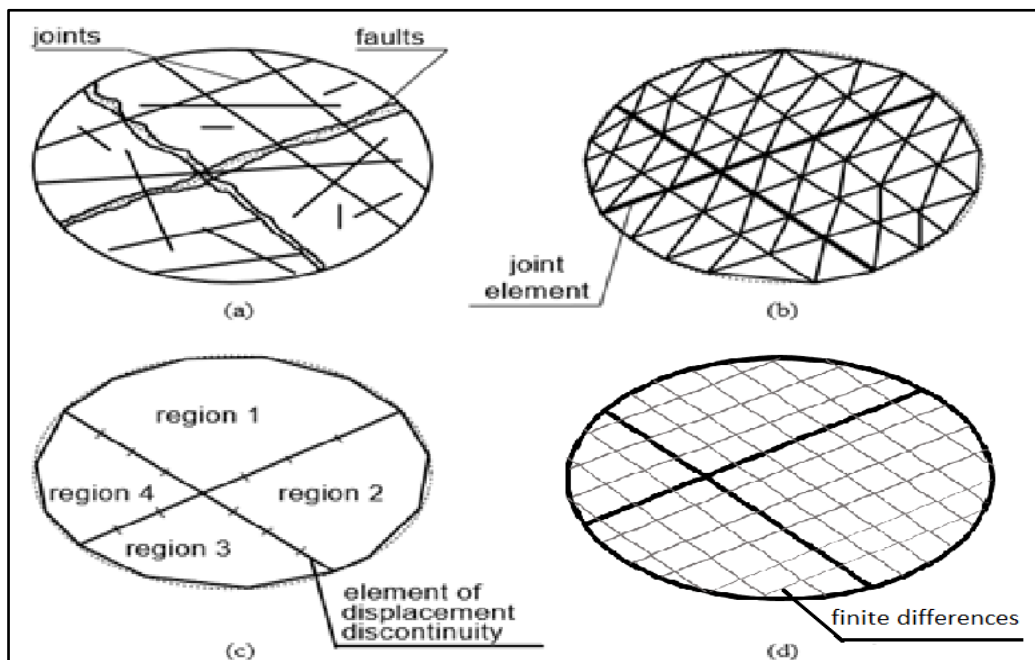
100 classical methods. The dynamic problems are solved by FDMs, where the
101 displacements are a function of time and position. In addition, maximum time
102 steps are required explicitly to ensure stability while solving dynamic problems
103 (Bobet, 2010). The localized formulation and its solution are more efficient for
104 memory storage and handling computer applications. There is no local trial in the
105 neighbourhood of sampling points to approximate PDE, as is concluded in FEM and
106 BEM. On the other hand, the conventional FDMs have several shortcomings such
107 as material heterogeneity, complicated boundary conditions, and inflexibility in
108 dealing with fractures (Shojaei et al., 2019; Wang, 2020). In general, the FDMs
109 are incompatible for modelling rock mechanics problems (Nikolić et al., 2016).

110 The finite element method (FEM) is the most widely employed numerical approach
111 for the analysis of the continuous or quasi continuous media across the science
112 and engineering fields. The term of "Finite Elements" was firstly introduced by
113 Clough (1960). The continuum is discretised into the small-scale aspects in the
114 FEMs. Finite element method (FEM) has proved to be successful in distinct
115 applications for solving geomechanical problems numerically. The indigenous
116 governing equations of geomechanics can convey the various formulations, and
117 the distinct formulation can be expanded, based on the finite element method.
118 The benefit of this approach is that the result is guaranteed to be the exact solution
119 as a result of the discrepancy formulation, which is mathematically identical to the
120 original equation (Zhao 2012). In general, there are well-established numerical
121 methods for solving geomechanical problems. The finite element method (FEM) is
122 the most common and widely implemented due to its flexibility in handling material
123 characterisations of heterogeneity, nonlinearity, and boundary conditions.

124 However, it is computationally challenging for dynamic related problems (Bobet,
125 2010). Compared to the FDM, the FEM covers enough flexibility in dealing with
126 fractures, complicated boundary conditions, the treatment of the material
127 heterogeneity, nonlinear deformation, in situ stress, and gravity (Jing and Hudson,
128 2002). The most significant shortcoming factors are the treatment of the fractures
129 and fracture growth in the implantation of the FEM for the rock mechanics
130 problems. The fracture elements cannot be torn in the general continuum
131 hypothesis during the FEM implementations. Therefore, the FEM suffers from the
132 treatment of block rotation, entire detachment, and large-scale fracture opening
133 (Manouchehrian et al., 2012). The FEM is disabled while the simulation process of
134 the fracture growth due to the required small element sizes, fracture growth
135 continuous re-meshing, and convenient fracture path and element edges. This
136 disadvantage makes the FEM less efficient than the boundary element method
137 (BEM) in dealing with fracture problems (Dadas, 2020; Jing, 2003)

138 The boundaries of the continuum are discretised only in the boundary element
139 method (BEM), whereas the complete domain needs to be discretized in the FDM
140 and FEM methods (Jing and Hudson, 2002; Manouchehrian et al., 2012). In
141 addition, there is no artificial boundaries are required where the common problems
142 in geomechanics are the extended medium to infinity, while the artificial
143 boundaries are required in both FDM and FEM methods (Fahmy, 2021; Mesquita
144 and Pavanello, 2005). BEMs are especially convenient to address the static
145 continuum problems with small boundary to volume ratios, with stress and elastic
146 behaviour or displacements implemented to the boundaries (Gao, 2003). Also, the
147 BEM has much simpler mesh generation and input data preparation with the

148 reduction of the model dimension by one compared with the FDM and FEM (Jing,
149 2003). Furthermore, the continuous domain inside is applied as a solution, unlike
150 the discontinuous point-wise solution is determined using FDM and FEM.
151 Nonetheless, the BEM is not so sufficient in dealing with material heterogeneity,
152 compared to the FEM because BEM cannot involve as many subdomains as
153 elements in the FEM. Also, the BEM is not powerful in simulating the nonlinear
154 material behaviour compared to the FEM such as in plasticity and damage growth
155 process (Bobet, 2010; Jing and Hudson, 2002). In general, the BEM is more
156 applicable for solving problems of fracturing inhomogeneous and linearly elastic
157 bodies (Kabele et al., 1999). Fig. 10 presents the discretization concepts of finite
158 element methods (FEM), boundary element method (BEM), and finite difference
159 method for fractured systems.



160

161
162
163

Fig. 10. Illustration of the discretization concepts as (a) shows the representation of the fractured rock mass (b) shows the finite element method (FEM) concept, (c) represents the boundary element method (BEM) concept, and (d) demonstrates the discrete element method (DEM) concept (After Jing, 2003).

164 5.2.1 Discontinuum Approaches

165 The discontinuum approach consists of the discrete/distinct element method
166 (DEM) with an explicit solution form and distinct deformation analysis (DDA) with
167 an implicit solution scheme. The discontinuum modelling represents the fractured
168 rock as an assemblage of blocks bounded by a number of intersecting
169 discontinuities (Lei et al., 2017; Lisjak and Grasselli, 2014). The mechanical
170 computation of the fractured geometry can be treated as rigid bodies or
171 deformable subdomains.

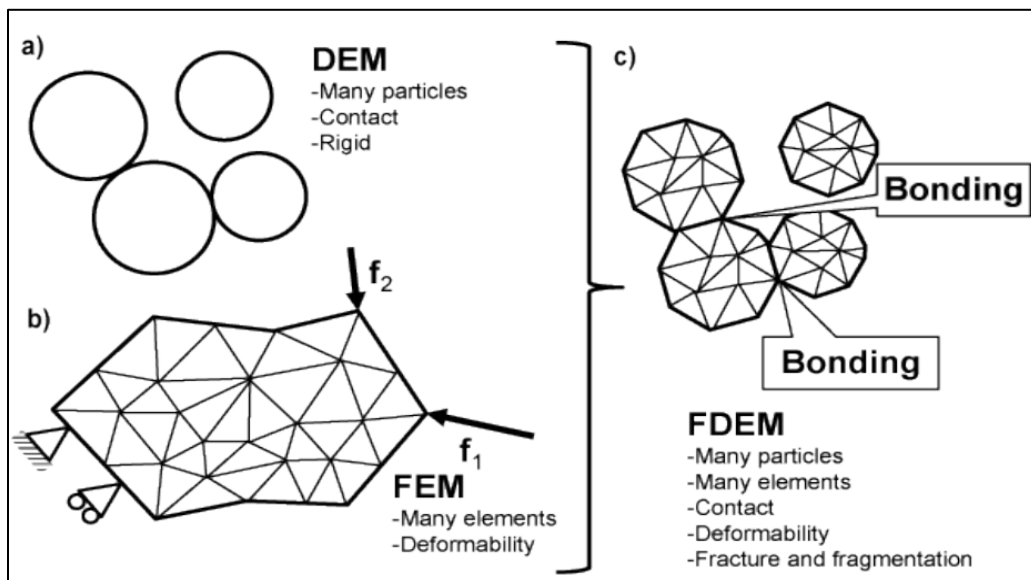
172 The distinct element method (DEM) was originally identified by Cundall (1988).
173 The DEM computation procedures are basically involved (1) the contact between
174 blocks and the contact forces between distinct bodies that are computed based
175 on their relative problems, (2) Newton's second law to calculate acceleration for
176 each distinct element, (3) the velocity and displacement are further developed by
177 time integration with new positions obtained (Hatzor, 2008). The DEM is
178 implemented under an explicit time scheme to solve the problems iteratively until
179 the complement of the block interaction process simulation. Despite the possibility
180 of using a DEM code to model the continuum, the main advantage of the DEM is
181 to model the discontinuities through specific constitutive relations (André et al.,
182 2012). Nonetheless, the proper simulation of the continuous geomechanical
183 materials is the main difficulty for DEM. Although the simulations of the
184 geomechanical problems are simple and accurate, they might need too much
185 computational time for the current computational technology (Ferretti, 2020).
186 Unlike continuous FEM, the DEM can handle the stress-strain characteristics of

187 intact rocks, the shearing/opening of preexisting fractures, the interaction
188 between multiple fractures and blocks (Lei et al., 2017).

189 The discontinuous deformation analysis is developed to capture the deformation
190 and motion of multi block systems by Shi and Goodman (1985, 1989). Although
191 the discretization method is quite the same for both DEM and DDA, the basic
192 differences between DEM and DDA lies to the computational framework. The DEM
193 employs explicit solution scheme to deal with each blocks separately, whereas the
194 DDA applies the implicit solution form to calculate the displacement field based on
195 a minimization of the whole blocky domain of the potential energy. Compared to
196 the DEM approach, the DDA approach has a significant advantage for fast
197 convergence with unconditional numerical stability that needs a time step smaller
198 than the critical threshold (Jing, 2003).

199 It is worth mentioning that several efforts have done to combine the finite element
200 analysis of stress/deformation evolution with the discrete element solutions of
201 transient dynamics, contact detection, and interactions in terms of the hybrid finite
202 element- discrete element method (FDEM) (An et al., 2021; Knight et al., 2020;
203 A Lisjak and Grasselli, 2014; Munjiza, 2004). In this discontinuum solution form,
204 the FEM approach is employed to capture the internal stress field of each discrete
205 matrix block while the DEM algorithm is used to calculate the translation, rotation,
206 and interaction of multiple rock blocks (Munjiza, 2004). Fig. 11(b) shows the
207 process of discretization for the solid bodies into a number of elements that deform
208 in accordance with the prescribed boundary and loading conditions using the FEM.
209 On the other hand, the original of the DEM deals with a large number of rigid

210 particles that interact with each other through contact and cohesion laws as shown
211 in Fig. 11(a). When these techniques of FEM and DEM are coupled, the solid bodies
212 are modeled as an assemblage of deformable particles that are bonded with each
213 other as depicted in Fig. 11(c). A series of cohesion points are employed to
214 represent the particle bonds numerically that is located along the boundaries of
215 the deformable particles (Fiore et al., 2013).



216

217 *Fig. 11. Illustration of the main feature of the combined finite element method and distinct element method (Fiore et al.,*
218 *2013).*

219

220

221

222

223

224

225 6.0 Coupled Geomechanics and Fluid Flow

226 The dynamic coupling of geomechanics and fluid flow is of interest in many areas
227 of science and engineering (Minkoff et al., 2003). Coupling geomechanics and fluid
228 flow have received a great deal of attention in civil and geotechnical engineering
229 for many years (Majorana et al., 2015; McCartney et al., 2016). As a result of the
230 shrinkage and extension of structural deformation, coupled structural mechanics
231 and heat flow also have been investigated in structural science and mechanical
232 engineering (Baran et al., 2017).

233 In the petroleum engineering discipline, coupled fluid flow and geomechanical
234 interactions can play a major role in dictating the behaviour of fluid flow in
235 fractures and tight rock reservoirs. The characterisation of reservoir geomechanics
236 can play a critical role in enhanced oil recovery (Chiaramonte et al., 2011; Guy et
237 al., 2012), subsidence, stability of wells (Fjær et al., 2008), stress-dependent
238 porosity, the permeability of rock matrix and stress-dependent fracture aperture
239 change (Cao et al., 2019; Mohiuddin et al., 2000; Sanaee et al., 2012) in fractured
240 and unconventional reservoirs. Wellbore stability problems have been the subject
241 of several studies due to the vicinity changes of the stress and strain around the
242 wellbore (Zoback, 2007). Reservoir compaction may lead to serious damage in the
243 wellbore during surface subsidence as a result of reservoir pressure depletion, but
244 can also increase oil recovery and the slow decline in reservoir pressure while
245 production takes place (Muggeridge et al., 2014; Pettersen, 2010).

246 6.1 Coupling Schemes

247 Several coupling schemes have been used to model geomechanics and fluid flow
248 interactions (Ahmed and Al-Jawad, 2020; Curnow and Tutuncu, 2015; Doster and
249 Nordbotten, 2015; Jing, 2003; Kim et al., 2013; Lavrov, 2017; Longuemare et al.,
250 2002; Rutqvist and Stephansson, 2003; Sanaee et al., 2013; Weishaupt et al.,
251 2019; Xiong et al., 2011; Zhao et al., 2017). Coupling methods are generally
252 divided into two different categories: volume coupling and coupling through flow
253 properties (Settari and Mourits, 1998). Volume coupling requires the same pore
254 volume changes in reservoir geomechanics and flow models which are the
255 functions of stress, pressure, and temperature (Lee and Schechter 2015). In the
256 coupling through flow properties, permeability and relative permeability are varied
257 as a result of changes in stress and displacements (Settari and Mourits, 1998).

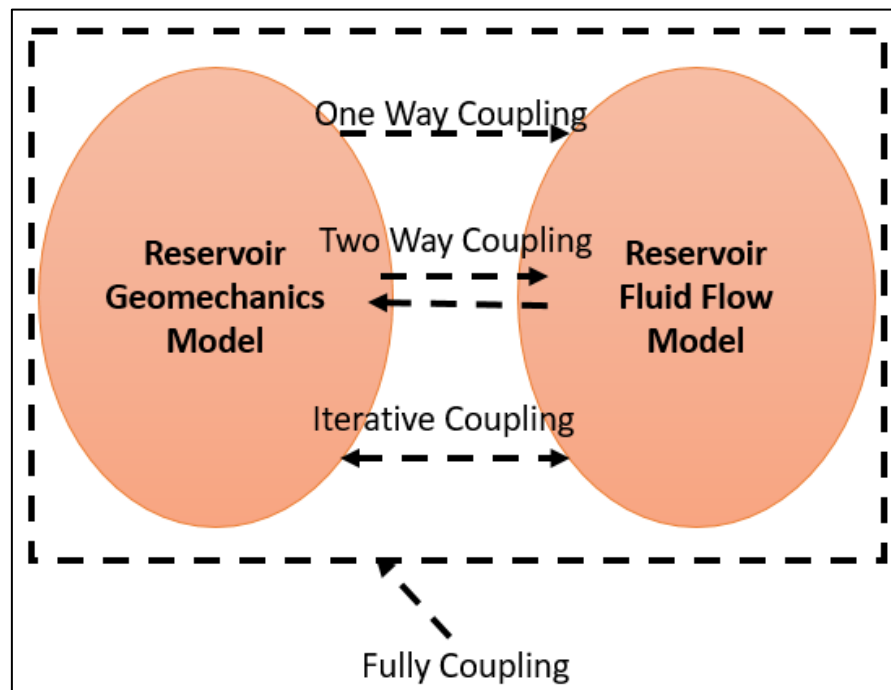
258 Furthermore, methods of coupling between geomechanics (solid deformation) and
259 reservoir flow, in mathematical terms, are generally categorized into four types:
260 one-way coupling, two-way coupling, iteratively coupling and fully coupling (Tran
261 et al., 2004).

262 1. One-way coupling: In one-way coupling schemes, two separate essential sets
263 of equations are solved independently for fluid flow and geomechanical
264 deformation over the same time period (Minkoff et al., 2003). This type of
265 coupling is also called explicit coupling because the data is merely conveyed in
266 a one-way direction from a fluid flow simulator to a geomechanical model. This
267 means that changes in pore pressure lead to changes in stress, strains, and
268 displacements, but changes in stress and strain do not impact the pore

269 pressure changes (Tran et al., 2004). Although there is the weakest link
270 between geomechanical deformation and fluid flow (Tran et al., 2004), one-
271 way coupling has provided valuable insight into a physical situation, and it is
272 obviously desirable for fluid flow alone, where the mechanical situation is
273 important (Minkoff et al., 2003). For instance, a one-way coupling experiment
274 was employed successfully that involved 200 fluid flow simulations to predict
275 well failure rates in the Belridge Field, California (Fredrich et al., 2000, 1996).
276 Although the numerical modelling of one-way coupling is simple and does not
277 require the magnificent development for the modelling of field scale, the one-
278 way coupling is less desirable from the physical point of view compared to the
279 other types of coupling (Fredrich et al., 2000).

280 2. Two-way coupling: The fundamental concept of two-way coupling is an
281 extension of one-way coupling and sometimes called loose coupling or pseudo-
282 coupling (Chin et al., 2002; Tran et al., 2004). In two-way coupling, reservoir
283 geomechanics and fluid flow simulators are run sequentially (Jin et al., 2000)
284 based on two distinct sets of equations that are solved independently, and the
285 information is conveyed in both directions between the two simulators (Minkoff
286 et al., 2003). Two-way coupling is relatively as simple as one-way coupling,
287 but its main advantage is the fact that it captures much more non-linear physics
288 between geomechanical and reservoir flow simulators, very close to fully
289 coupling (Dubinya et al., 2015; Kim et al., 2012). The primary drawback of
290 explicit coupled schemes (one-way and two-way coupling) is that the explicit
291 nature of the coupling can enforce time step restrictions on runs because of

292 concerns about stability and accuracy (Dean et al., 2006). Fig.12 defines how
293 distinct numerical coupling schemes work.



294
295 *Fig. 12. Representation of various types of simulation coupling schemes.*

296 3. Iterative coupling: In this type of coupling, either reservoir flow variables or
297 geomechanics variables are solved first, and then the other variables are solved
298 sequentially at each time step iteration (Lee and Schechter 2015; Tran, Settari,
299 and Nghiem 2004). The governing equations of the flow simulator and
300 reservoir geomechanics model subsystems are decomposed by a coupled
301 system of equations. While the reservoir flow simulator and geomechanics
302 model solve their governing subsystems of equations separately, the coupled
303 system of equations is solved iteratively using data variables between both
304 subsystems as shown on the lower part of Fig.13, through a data exchange
305 interface (Chin et al., 2002). The main advantages of iterative coupling is the
306 privilege that they are easy to implement between an existing reservoir flow

307 simulator and geomechanics model through a data exchange interface (Mikelić
308 et al., 2014). The primary shortcoming to the iteratively coupling scheme is
309 the display of the first-order convergence rate calculation in the nonlinear
310 iterations and then may require a huge number of iterations for complex issues
311 (Cervera et al., 1996; Dean et al., 2006).

312 4. Fully coupling: the governing equations of reservoir flow variables (such as
313 saturation, pressure, and temperature) and the geomechanical response (such
314 as displacements) are solved simultaneously (Charoenwongsa et al., 2010;
315 Giani et al., 2018; Pan et al., 2009, 2007; Settari and Walters, 2001; Stone et
316 al., 2000). This coupling scheme is sometimes referred to as an implicit
317 coupling, because the whole system is calculated simultaneously and can be
318 discretized on one grid domain (Tran et al., 2004), as depicted on the upper
319 part of Fig. 13. The advantage of a fully coupling approach is internal
320 consistency and the accuracy of the solution (Giani et al. 2018; Yang, Moridis,
321 and Blasingame 2014). Another advantage of the fully coupling approach is the
322 stability and also conservation of the second-order convergence for non-linear
323 iterations. However, the coupling of flow and geomechanics conservative
324 relations are complicated to adopt and modelling of the fully coupling
325 multiphase flow simulator is extraordinarily difficult to models of inelastic
326 mechanical deformation and nonlinear (Minkoff et al., 2003; Osorio and Chen,
327 1999). In addition, the fully coupling approach requires more code
328 development techniques, becomes slower than other approaches, and requires
329 utilisation of iterative methods in some situations (Rocca, 2009).

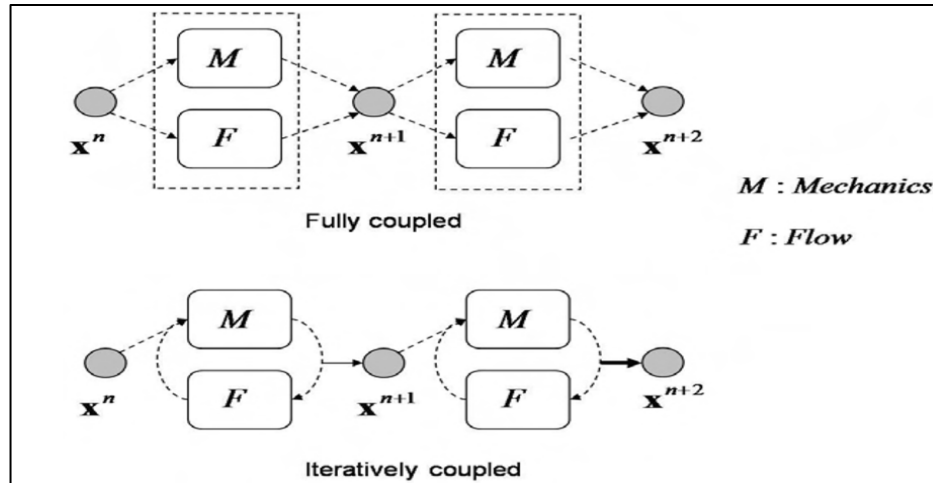


Fig. 13. Schematics of fully and iterative coupling methods (Kim, 2010).

330

331

332 6.2 Numerical Discretization

333 Discretization is used to transfer the mathematical model into an algebraic
 334 equation system or numerical model (Liu, 2018). The main principle of
 335 discretization is to divide the whole domain of the reservoir into a number of
 336 discrete subdomains (elements and control volumes), each of which is represented
 337 by a discrete number of points (grids, nodes) (Nordbotten et al., 2019).
 338 Subsequently, the objectives of discretization is to convert partial differential
 339 equations into a set of algebraic equations which are valid at each of these discrete
 340 points (grid points, nodes), followed by solving the system of the algebraic
 341 equation to determine the values of the dependent variables at each of the discrete
 342 points that cannot be solved analytically (BinZubair et al., 2010).

343 Several distinct temporal and spatial discretization methods are employed in the
 344 literature for coupling reservoir geomechanics and fluid flow in fractured porous
 345 media. The first order differential equation method is applied for temporal
 346 discretization, while various distinct methods are employed for spatial

347 discretization, such as the finite difference method (FDM), finite element method
348 (FEM), finite volume method (FVM), and so on.

349 a) Review of Reservoir Geomechanics Discretization

350 In fractured geomechanical modelling, the finite element methods are
351 widely employed by nodal enrichment for the discontinuous displacement
352 modes (Ren et al., 2018). Although finite difference methods are often
353 applied to special cases of one-dimensional problems, such as the simplified
354 geometries of crystal layers, finite element methods are more applicable to
355 a multidimensional differential equation with complicated geometries
356 (Saikia et al., 2018). To capture displacement discontinuity jumps in the
357 fractured porous rocks, finite element methods are enhanced with some
358 local degree of freedom, the outcome of which is referred to as the
359 embedded finite element method (EFEM). Alternatively, the hypothesis of
360 partition unity is employed in the extended finite element method (XFEM),
361 with nodal enrichment used to capture the various feature of fractured
362 porous media discontinuity (Armero and Linder, 2008). Oliver, Huespe, and
363 Sánchez (2006) (Oliver et al., 2006) compared EFEM and XFEM, with an
364 emphasis on accuracy and computational cost. However, it is demonstrated
365 that both approaches present the same quantitative and qualitative results
366 for enough refined meshes. In general, EFEM showed higher accuracy and
367 relatively lower cost than XFEM (Oliver et al., 2006).

368 b) Review of Fluid Flow Discretization

369 Extended finite element methods (XFEM) are also used to solve the single
370 and two-phase flow in the fractured reservoirs and is less recommended to
371 model coupled fluid flow and geomechanics compared to other methods
372 (Boon et al., 2018; Fumagalli and Scotti, 2013). Despite their simplicity,
373 finite difference methods (FDM) are also applied to solve fluid flow in
374 fractured reservoirs with the aid of other discretization methods (Antonietti
375 et al., 2016). In addition, the finite volume methods are used to capture
376 the degree of freedom of more physical unknowns that may exist in the
377 centre of the matrix blocks, and also to capture fracture discontinuities for
378 multiphase flow, based on the discrete fracture matrix models (Stefansson
379 et al., 2018). The main advantages of finite volume methods are that they
380 preserve the locality of mass conservation as well as computational
381 efficiency and flexibility (Ahn, 2019; Profito et al., 2015; X. Yang et al.,
382 2020).

383 c) Review of Coupled Reservoir Geomechanics and Fluid Flow Discretization

384 Extensive amount of research has focused on implementing various
385 discretization schemes based on the length scale of the problems and
386 coupling schemes (Chin et al., 2002; Duran et al., 2020; Garipov et al.,
387 2016; Garipov and Hui, 2018; Jalali and Dusseault, 2012; Minkoff et al.,
388 2003) as listed in Table 2. There is a lack of physical control in the fracture
389 subdomain due to the use of the Darcy flow equation. Researchers (Ren et
390 al., 2018) also highlighted the coupling between reservoir geomechanics
391 and two-phase flow using the extended element method (XFEM) and finite

392 volume (FVM) discretization based on the discrete fracture matrix model. It
393 is noted that no literature has been published on coupling reservoir
394 geomechanics using FEM, and multiphase flow using FVM, for non-Darcy
395 flow equations in the fracture subdomain though.

Table 2: Comparison of distinct coupling and discretization schemes.

Type of Coupling	Fluid Phases	Discretization Method		Flow Domain
		Flow	Geomechanics	
Two-way coupling (Minkoff et al., 2003)	Two Phase	FEM	FEM	Full Domain
Fully coupling (Garipov et al., 2016)	Single Phase	FVM	FEM	Full Domain
Fully Coupling (Yang, Moridis, and Blasingame 2014)	Two Phase	FEM	FEM	Full domain
Iterative Coupling (Chin et al., 2002)	Two Phase	XFEM	XFEM	Full Domain
Iterative Coupling (Duran et al., 2020)	Single Phase	FEM	FEM	Full Domain

398 7.0 Concluding Remarks

399 In this review, the most recent mathematical, numerical, and discretization
400 approaches for reservoir geomechanics and fluid flow are investigated. Various
401 types of coupling schemes are described and compared, related to their
402 application, computational efficiency, and cost. The available literature has shown,
403 in terms of modelling and simulation, there is mature research in the field for the
404 single-phase flow in fractured porous media. The remaining challenges for fluid
405 flow are the suitable selection of the conceptual models for the flow governing
406 equations, and the necessity of the upscaling procedure and discretization in the
407 fracture network. This is particularly important in capturing the fluid properties in
408 the fractures and the surrounded porous matrix. In contrast, if the local fracture
409 networks play as the dominant flow path in the area of interest, the fractures must
410 be represented explicitly; in such cases, DFN and DFM are the most preferable
411 methods to capture the flow characteristics in the fracture and the surrounded
412 porous media. The dual continuum approach is conceptually simpler and
413 computationally much less demanding than the DFN and DFM approaches (Kumar
414 et al., 2016). In addition, modelling purposes and the quality of the data in the
415 specific application are major influencing parameters used to select the proper
416 modelling schemes.

417 Multiphase flow occasionally occurs in many applications including the fractured
418 porous media. This complex type of flow is governed by many physical parameters,
419 such as saturation, wettability, relative permeability, and capillary pressure, and
420 subsequently causes non-linearly coupled flow. The experimental and numerical
421 multiphase flow data in fractured porous media context is exceptionally sparse for
422 the constitutive relations of relative permeability and capillary pressure, compared
423 to the non-fractured porous media. Nonetheless, significant signs of progress have
424 been achieved to model multiphase flow in the fractured porous media (Helmig et
425 al., 2013; Sabti et al., 2016) since the first multiphase experimental (Kazemi and
426 Merrill, 1979) and numerical modelling work (Wu 2016). In addition, as a result of
427 having distinct relative permeability and capillary pressure in the constitutive
428 relations at the fracture and matrix interface in the fractured porous media, these
429 strong heterogeneities in the capillary barriers and resistance of flow leads to the
430 main numerical challenges (Antonietti et al., 2016; Brenner et al., 2018). Despite
431 several studies, modelling of multiphase flow is still an active area of research in
432 fractured porous media, in terms of the conceptual and constitutive relations of
433 multiphase flow, conventional mathematics and numerical representation of
434 multiphase Darcy law in fractured rocks (Berre et al., 2019).

435 There is a strong relationship between fractured flow patterns and fracture
436 structure itself. As a result of fluid flow processes, the fracture characteristic
437 configurations change, and then the fracture deformations affect the fluid flow
438 indirectly in the fractured porous media. Therefore, several kinds of coupling
439 schemes have been used to couple reservoir geomechanics characteristics and
440 fluid flow in the fractured porous media (Jiang and Yang, 2018; Rutqvist and

441 Stephansson, 2003; Xue et al., 2014). One-way coupling is widely used for
442 subsidence analysis, because it is more straight forward and less expensive, while
443 it has a lower degree of coupling compared to other coupling methods (Angus et
444 al., 2015; Giani et al., 2018). Two-way coupling is far more appropriate than one-
445 way coupling to predict flow behaviour in fractured reservoirs (Kim et al. 2012).
446 Despite a high resolution of results and convergence, a fully coupled method
447 requires a unified hydromechanical simulator to provide sufficient definition for
448 both reservoir geomechanics and fluid flow compared to iterative coupling scheme
449 (Ashworth and Doster, 2019; Zareidarmiyan et al., 2018). In addition, the fully
450 coupled scheme requires enormous software development efforts and large
451 computational costs (Kim et al., 2013) whereas the iterative coupling scheme
452 combines the conventional reservoir geomechanics and fluid flow simulators
453 through a data exchange interface (Chin et al., 2002). Despite several research
454 efforts (Ashworth and Doster, 2019; Martin et al., 2017; Weishaupt et al., 2019),
455 coupled geomechanics and multiphase flow is still a challenging issue related to
456 mathematical, numerical models and discretization schemes to capture the
457 hydrodynamic behaviours, such as fracture deformation and fluid flow interaction
458 at fracture matrix interface in naturally fractured reservoirs.

459

460

461

462 Nomenclature and units

463 P = Effective confining pressure, $MPa = \frac{N}{m^2}$

464 p = Pore pressure, MPa

465 σ_n = Effective normal stress, MPa

466 K = Bulk modulus of the material, MPa

467 ε_v = Volumetric strain

468 u = Velocity, m/s

469 G = Shear modulus of the material, GPa

470 v = Darcy velocity, m/s

471 k = Effective permeability of the rock, m^2

472 μ = Viscosity of the fluid, $Pa.s$

473 ρ = Density of the fluid, kg/m^3

474 g = gravitational acceleration, m/s^2

475 D = Depth of the datum, m

476 φ = Porosity of the rock, *fraction*

477 q = Source term, $kg/m^2.s$

478 k_a = Absolute permeability, m^2

479 k_r = Relative permeability, *fraction*

480 β = Subscript of the phases ($\beta = g$ for gas, $\beta = w$ for water, and $\beta = o$ for oil)

481 S = Saturation of the fluid, *fraction*

482 P_c = Capillary pressure, Pa

483 P_w = Pressure of wetting fluid, Pa

484 P_n = Pressure of non-wetting fluid, Pa

485 λ = Mobility of the fluid, *dimensionless*

486 c = Consolidation coefficient

487 l = Length of the sample, m
488 σ = Total stress, MPa
489 σ' = Effective stress, MPa
490 δ = Kronecker delta
491 α = Biot Willis Coefficient, *fraction*
492 K_d = Drained bulk moduli of the material, MPa
493 K_s = Solid bulk moduli of the material, MPa

494
495
496
497
498
499
500
501
502
503
504
505
506
507
508
509
510
511
512

513 References

- 514 Aavatsmark, I., Barkve, T., Bøe, O., Mannseth, T., 1996. Discretization on non-orthogonal, quadrilateral
515 grids for inhomogeneous, anisotropic media. *J. Comput. Phys.* 127, 2–14.
516 <https://doi.org/10.1006/jcph.1996.0154>
- 517 Aavatsmark, I., Barkve, T., Mannseth, T., 1998. Control-Volume Discretization Methods for 3D
518 Quadrilateral Grids in Inhomogeneous, Anisotropic Reservoirs. *SPE J.* 3, 146–149.
519 <https://doi.org/10.2118/38000-pa>
- 520 Aavatsmark, I., Eigestad, G.T., Heimsund, B.O., Mallison, B.T., Nordbotten, J.M., Øian, E., 2010. A new
521 finite-volume approach to efficient discretization on challenging grids. *SPE J.* 15, 658–669.
522 <https://doi.org/10.2118/106435-PA>
- 523 Aavatsmark, I., Eigestad, G.T., Mallison, B.T., Nordbotten, J.M., 2008. A Compact Multipoint Flux
524 Approximation Method with Improved Robustness. *Numer. Methods Partial Differ. Equ.* 32, 1329–
525 1360. <https://doi.org/https://doi.org/10.1002/num.20320>
- 526 Abass, H.H., Ortiz, I., Khan, M.R., Beresky, J.K., Sierra, L., 2007. Understanding Stress Dependant
527 Permeability of Matrix, Natural Fractures, and Hydraulic Fractures in Carbonate Formations, in:
528 Society of Petroleum Engineers - SPE Saudi Arabia Section Technical Symposium 2007. Society of
529 Petroleum Engineers, Dhahran, Saudi Arabia. <https://doi.org/https://doi.org/10.2118/110973-MS>
- 530 Abbas, F., 2000. Recovery Mechanisms in Fractured Reservoirs and Field Performance. *J. Can. Pet.*
531 *Technol.* 39, 13–17. <https://doi.org/https://doi.org/10.2118/00-11-DAS>
- 532 Ahmed, B.I., Al-Jawad, M.S., 2020. Geomechanical modelling and two-way coupling simulation for
533 carbonate gas reservoir. *J. Pet. Explor. Prod. Technol.* 10, 3619–3648.
534 <https://doi.org/10.1007/s13202-020-00965-7>
- 535 Ahn, S., 2019. Computing the Distribution: Adaptive Finite Volume Methods for Economic Models with
536 Heterogeneous Agents. Oslo.
- 537 An, H., Song, Y., Liu, H., Han, H., 2021. Combined Finite-Discrete Element Modelling of Dynamic Rock
538 Fracture and Fragmentation during Mining Production Process by Blast. *Hindawi* 2021.
539 <https://doi.org/https://doi.org/10.1155/2021/6622926>
- 540 André, D., Iordanoff, I., Charles, J.L., Néauport, J., 2012. Discrete element method to simulate
541 continuous material by using the cohesive beam model. *Comput. Methods Appl. Mech. Eng.* 213–
542 216, 113–125. <https://doi.org/10.1016/j.cma.2011.12.002>
- 543 Angus, D.A., Dutko, M., Kristiansen, T.G., Fisher, Q.J., Kendall, J.M., Baird, A.F., Verdon, J.P., Barkved,
544 O.I., Yu, J., Zhao, S., 2015. Integrated hydro-mechanical and seismic modelling of the Valhall
545 reservoir: A case study of predicting subsidence, AVOA and microseismicity. *Geomech. Energy*
546 *Environ.* 2, 32–44. <https://doi.org/10.1016/j.gete.2015.05.002>
- 547 Antonietti, P.F., Formaggia, L., Scotti, A., Verani, M., Verzott, N., 2016. Mimetic finite difference
548 approximation of flows in fractured porous media. *ESAIM Math. Model. Numer. Anal.* 50, 809–832.
549 <https://doi.org/10.1051/m2an/2015087>
- 550 Armero, F., Linder, C., 2008. New finite elements with embedded strong discontinuities in the finite
551 deformation range. *Comput. Methods Appl. Mech. Eng.* 197, 3138–3170.

- 552 <https://doi.org/10.1016/j.cma.2008.02.021>
- 553 Arrarás, A., Portero, L., Jorge, J.C., 2010. Convergence of fractional step mimetic finite difference
554 discretizations for semilinear parabolic problems. *Appl. Numer. Math.* 60, 473–485.
555 <https://doi.org/10.1016/j.apnum.2009.10.007>
- 556 Ashworth, M., Doster, F., 2019. An Open Source Numerical Framework for Dual-Continuum
557 Geomechanical Simulation, in: *Society of Petroleum Engineers - SPE Reservoir Simulation*
558 *Conference 2019, RSC 2019. Society of Petroleum Engineers, Galveston, Texas, USA.*
559 <https://doi.org/https://doi.org/10.2118/193846-MS>
- 560 Baca, R.G., Arnett, R.C., Langford, D.W., 1984. Modelling fluid flow in fractured-porous rock masses by
561 finite-element techniques. *Int. J. Numer. Methods Fluids* 4, 337–348.
562 <https://doi.org/https://doi.org/10.1002/flid.1650040404>
- 563 Bagheri, M., Settari, A., 2005. Modeling of geomechanics in naturally fractured reservoirs. *SPE Reserv.*
564 *Simul. Symp. Proc.* 11, 235–246. <https://doi.org/SPE-93083-PA>
- 565 Bai, J., Sierra, L., Martysevich, V., 2019. Recompletion with Consideration of Depletion Effect in Naturally
566 Fractured Unconventional Reservoirs, in: *53rd U.S. Rock Mechanics/Geomechanics Symposium.*
567 *American Rock Mechanics Association, New York City, New York.* <https://doi.org/ARMA-2019-0321>
- 568 Baran, I., Cinar, K., Ersoy, N., Akkerman, R., Hattel, J.H., 2017. A Review on the Mechanical Modeling of
569 Composite Manufacturing Processes. *Arch. Comput. Methods Eng.* 24, 365–395.
570 <https://doi.org/https://doi.org/10.1007/s11831-016-9167-2>
- 571 Bars, M.L., Worster, M.G., 2006. Interfacial conditions between a pure fluid and a porous medium:
572 implications for binary alloy solidification. *J. Fluid Mech.* 550, 149–173.
573 <https://doi.org/10.1017/S0022112005007998>
- 574 Barton, C.A., Moos, D., Hartley, L., Baxter, S., Foulquier, L., Holl, H., Hogarth, R., 2013. Geomechanically
575 Coupled Simulation of Flow in Fractured Reservoirs, in: *Thirty-Eighth Workshop on Geothermal*
576 *Reservoir Engineering. Stanford University, Stanford, California, p. 12.*
- 577 Bear, J., 1972. *Dynamics of Fluids in Porous Media.* American Elsevier Publishing Company, New York
578 City, New York. <https://doi.org/10.2136/sssaj1973.03615995003700040004x>
- 579 Bemmer, E., Boutéca, M., Vincké, O., Hoteit, N., Ozanam, O., 2001. Poromechanics: from Linear to
580 Nonlinear Poroelasticity and Poroviscoelasticity. *Oil Gas Sci. Technol.* 56, 531–544.
581 <https://doi.org/https://doi.org/10.2516/ogst:2001043>
- 582 Berkowitz, B., 2002. Characterizing flow and transport in fractured geological media: A review. *Adv.*
583 *Water Resour.* 25, 861–884. [https://doi.org/10.1016/S0309-1708\(02\)00042-8](https://doi.org/10.1016/S0309-1708(02)00042-8)
- 584 Berndt, M., Lipnikov, K., Moulton, D., Shashkov, M., 2001. Convergence of mimetic finite difference
585 discretizations of the diffusion equation. *J. Numer. Math.* 9, 265–284.
586 <https://doi.org/10.1515/JNMA.2001.265>
- 587 Berre, I., Doster, F., Keilegavlen, E., 2019. Flow in Fractured Porous Media: A Review of Conceptual
588 Models and Discretization Approaches. *Transp. Porous Media* 130, 215–236.
589 <https://doi.org/10.1007/s11242-018-1171-6>
- 590 BinZubair, H., MacLachlan, S.P., Oosterlee, C.W., 2010. A geometric multigrid method based on L-shaped

591 coarsening for PDEs on stretched grids. Numer. Linear Algebr. with Appl. 17, 871–894.
592 <https://doi.org/10.1002/nla.665>

593 Biot, M.A., 1962. Mechanics of deformation and acoustic propagation in porous media. J. Appl. Phys. 33,
594 1482–1498. <https://doi.org/10.1063/1.1728759>

595 Biot, M.A., 1956. Theory of Propagation of Elastic Waves in a Fluid-Saturated Porous Solid. J. Acoust. Soc.
596 Am. 28, 168–178. <https://doi.org/10.1121/1.1908239>

597 Biot, M.A., 1941. General theory of three-dimensional consolidation. J. Appl. Phys. 12, 155–164.
598 <https://doi.org/https://doi.org/10.1063/1.1712886>

599 Blunt, M.J., 2001. Flow in porous media - Pore-network models and multiphase flow. Curr. Opin. Colloid
600 Interface Sci. 6, 197–207. [https://doi.org/10.1016/S1359-0294\(01\)00084-X](https://doi.org/10.1016/S1359-0294(01)00084-X)

601 Bobet, A., 2010. Numerical Methods in Geomechanics. Arab. J. Sci. Eng. 35, 27–48.
602 [https://doi.org/10.1016/0378-3839\(84\)90026-7](https://doi.org/10.1016/0378-3839(84)90026-7)

603 Boon, W.M., Nordbotten, J.A.N.M., Yotov, I., 2018. Robust Discretization of Flow in Fractured Porous
604 Media. SIAM J. Numer. Anal. 56, 2203–2233. <https://doi.org/10.1137/17M1139102>

605 Brenner, K., Hennicker, J., Masson, R., Samier, P., 2018. Hybrid-dimensional modelling of two-phase flow
606 through fractured porous media with enhanced matrix fracture transmission conditions. J. Comput.
607 Phys. 357, 100–124. <https://doi.org/10.1016/j.jcp.2017.12.003>

608 Cao, N., Lei, G., Dong, P., Li, H., Wu, Z., Li, Y., 2019. Stress-Dependent Permeability of Fractures in Tight
609 Reservoirs. Energies 12. <https://doi.org/10.3390/en12010117>

610 Cervera, M., Codina, R., Galindo, M., 1996. On the computational efficiency and implementation of
611 block-iterative algorithms for nonlinear coupled problems. Eng. Comput. (Swansea, Wales) 13, 4–
612 30. <https://doi.org/10.1108/026444409610128382>

613 Charoenwongsa, S., Kazemi, H., Miskimins, J., Fakcharoenphol, P., 2010. A Fully-Coupled Geomechanics
614 and Flow Model for Hydraulic Fracturing and Reservoir Engineering Applications, in: Canadian
615 Unconventional Resources and International Petroleum Conference 2010. Society of Petroleum
616 Engineers, Calgary, Alberta, Canada, pp. 1460–1490. <https://doi.org/10.2118/137497-ms>

617 Chen, Y., Mallison, B.T., Durlofsky, L.J., 2008. Nonlinear two-point flux approximation for modeling full-
618 tensor effects in subsurface flow simulations. Comput. Geosci. 12, 317–335.
619 <https://doi.org/10.1007/s10596-007-9067-5>

620 Chiamonte, L., Zoback, M., Friedmann, J., Stamp, V., Zahm, C., 2011. Fracture characterization and
621 fluid flow simulation with geomechanical constraints for a CO₂-EOR and sequestration project
622 Teapot Dome Oil Field, Wyoming, USA. Energy Procedia 4, 3973–3980.
623 <https://doi.org/10.1016/j.egypro.2011.02.337>

624 Chin, L.Y., Thomas, L.K., Sylte, J.E., Pierson, R.G., 2002. Iterative coupled analysis of geomechanics and
625 fluid flow for rock compaction in reservoir simulation. Oil Gas Sci. Technol. 57, 485–497.
626 <https://doi.org/10.2516/ogst:2002032>

627 Clough, R.W., 1960. The Finite Element Method in Plane Stress Analysis, in: 2nd ASCE Conference on
628 Electronic Computation. Pittsburgh Pa., pp. 345–378.

629 Council, 1996. Rock Fractures and Fluid Flow, Rock Fractures and Fluid Flow: Contemporary

- 630 Understanding and Applications. NATIONAL ACADEMY PRESS, Washington, D.C.
631 <https://doi.org/10.17226/2309>
- 632 Cundall, P.A., 1988. Formulation of a three-dimensional distinct element model-Part I. A scheme to
633 detect and represent contacts in a system composed of many polyhedral blocks. *Int. J. Rock Mech.*
634 *Min. Sci.* 25, 107–116. [https://doi.org/10.1016/0148-9062\(88\)92293-0](https://doi.org/10.1016/0148-9062(88)92293-0)
- 635 Curnow, J.S., Tutuncu, A.N., 2015. Coupled geomechanics and fluid flow model for production
636 optimization in naturally fractured shale reservoirs. *SEG Tech. Progr. Expand. Abstr.* 34, 399–403.
637 <https://doi.org/10.1190/segam2015-5928833.1>
- 638 Dadzie, S.K., Reese, J.M., McInnes, C.R., 2008. A continuum model of gas flows with localized density
639 variations. *Phys. A Stat. Mech. its Appl.* 387, 6079–6094.
640 <https://doi.org/10.1016/j.physa.2008.07.009>
- 641 Datas, A., 2020. ULTRA-HIGH TEMPERATURE THERMAL ENERGY STORAGE, TRANSFER AND CONVERSION,
642 Ultra-High Temperature Thermal Energy Storage, Transfer and Conversion. Woodhead Publishing.
643 <https://doi.org/https://doi.org/10.1016/C2019-0-00964-8>
- 644 Dean, R.H., Gai, X., Stone, C.M., Minkoff, S.E., 2006. A comparison of techniques for coupling porous
645 flow and geomechanics. *SPE J.* 11, 132–140. <https://doi.org/10.2118/79709-PA>
- 646 Dong, Z., Li, W., Lei, G., Wang, H., Wang, C., 2019. Embedded discrete fracture modeling as a method to
647 upscale permeability for fractured reservoirs. *Energies* 12. <https://doi.org/10.3390/en12050812>
- 648 Doster, F., Nordbotten, J.M., 2015. Full Pressure Coupling for Geo-mechanical Multi-phase Multi-
649 component Flow Simulations, in: *SPE Reservoir Simulation Symposium*. Society of Petroleum
650 Engineers, Houston, Texas, USA, pp. 742–753. <https://doi.org/SPE-173232-MS>
- 651 Droniou, J., 2014. Finite volume schemes for diffusion equations: Introduction to and review of modern
652 methods. *Math. Model. Methods Appl. Sci.* 24, 1575–1619.
653 <https://doi.org/10.1142/S0218202514400041>
- 654 Dubinya, N., Lukin, S., Chebyshev, I., 2015. Two-Way Coupled Geomechanical Analysis of Naturally
655 Fractured Oil Reservoir's Behavior Using Finite Element Method, in: *SPE Russian Petroleum*
656 *Technology Conference*. Society of Petroleum Engineers, Moscow, Russia. [https://doi.org/SPE-](https://doi.org/SPE-176631-MS)
657 [176631-MS](https://doi.org/SPE-176631-MS)
- 658 Duran, O., Manouchehr, S., Devloo, P., Santos, E., 2020. An enhanced sequential fully implicit scheme for
659 reservoir geomechanics.
- 660 Fahmy, M.A., 2021. A new boundary element algorithm for modeling and simulation of nonlinear
661 thermal stresses in micropolar FGA composites with temperature-dependent properties. *Adv.*
662 *Model. Simul. Eng. Sci.* 8. <https://doi.org/10.1186/s40323-021-00193-6>
- 663 Falode, O., Manuel, E., 2014. Wettability Effects on Capillary Pressure, Relative Permeability, and
664 Irreducible Saturation Using Porous Plate. *J. Pet. Eng.* 2014, 1–12.
665 <https://doi.org/10.1155/2014/465418>
- 666 Ferretti, E., 2020. DECM: A discrete element for multiscale modeling of composite materials using the
667 cell method. *Materials (Basel)*. 13. <https://doi.org/10.3390/ma13040880>
- 668 Figueiredo, B., Tsang, C.F., Rutqvist, J., Niemi, A., 2015. A study of changes in deep fractured rock

- 669 permeability due to coupled hydro-mechanical effects. *Int. J. Rock Mech. Min. Sci.* 79, 70–85.
670 <https://doi.org/10.1016/j.ijrmms.2015.08.011>
- 671 Fiore, M., Cacy, R., Jon, D., Allan, C., Earl, E., Casteel, E., Darnell, J., Michael, W., 2013. Proceedings of the
672 Workshop on the Structural Cracking of the Cupola of Santa Maria del Fiore. Los Alamos, New
673 Mexico. <https://doi.org/10.2172/1156847>
- 674 Fjær, E., Holt, R.M., Horsrud, P., Raeen, A.M., Risens, R., 2008. *PETROLEUM RELATED ROCK MECHANICS*,
675 2nd ed. Elsevier B.V. [https://doi.org/10.1016/0148-9062\(93\)92632-Z](https://doi.org/10.1016/0148-9062(93)92632-Z)
- 676 Fleishmann, P., Kosik, R., Selberherr, S., 1999. Simple Mesh Examples to Illustrate Specific Finite Element
677 Mesh Requirements, in: 8th Int. Meshing Roundtable. Institute for Microelectronics, South Lake
678 Tahoe, CA, USA, pp. 241–246.
- 679 Fredrich, J.T., Arguello, J.G., Deitrick, G.L., De Rouffignac, E.P., 2000. Geomechanical Modeling of
680 Reservoir Compaction, Surface Subsidence, and Casing Damage at the Belridge Diatomite Field. *SPE*
681 *Reserv. Eval. Eng.* 3, 348–359. <https://doi.org/10.2118/65354-PA>
- 682 Fredrich, J.T., Arguello, J.G., Thorne, B.J., Wawersik, W.R., Deitrick, G.L., de Rouffignac, E.P., Myer, L.R.,
683 Bruno, M.S., 1996. Three-Dimensional Geomechanical Simulation of Reservoir Compaction and
684 Implications for Well Failures in the Belridge Diatomite, in: *SPE Annual Technical Conference and*
685 *Exhibition*. Society of Petroleum Engineers, Denver, Colorado, pp. 13–28.
686 <https://doi.org/10.2523/36698-ms>
- 687 Fumagalli, A., Scotti, A., 2013. A numerical method for two-phase flow in fractured porous media with
688 non-matching grids. *Adv. Water Resour.* 62, 454–464.
689 <https://doi.org/10.1016/j.advwatres.2013.04.001>
- 690 Gao, X.W., 2003. Boundary element analysis in thermoelasticity with and without internal cells. *Int. J.*
691 *Numer. Methods Eng.* 57, 975–990. <https://doi.org/10.1002/nme.715>
- 692 Garg, S.K., Nur, A., 1973. Effective Stress Laws for Fluid-Saturated Porous Rocks. *J. Geophys. Res.* 78,
693 5911–5921. <https://doi.org/10.1029/jb078i026p05911>
- 694 Garipov, T.T., Hui, M., 2018. Simulation of coupled geomechanics and multiphase flow in naturally
695 fractured reservoirs, in: 52nd U.S. Rock Mechanics/Geomechanics Symposium. American Rock
696 Mechanics Association, Seattle, Washington. <https://doi.org/ARMA-2018-1230>
- 697 Garipov, T.T., Karimi-Fard, M., Tchelepi, H.A., 2016. Discrete fracture model for coupled flow and
698 geomechanics. *Comput. Geosci.* 20, 149–160. <https://doi.org/10.1007/s10596-015-9554-z>
- 699 Geiger, S., Matthäi, S., Niessner, J., Helmig, R., 2009. Black-Oil Simulations for Three-Component, Three-
700 Phase Flow in Fractured Porous Media. *SPE J.* 14, 338–354. <https://doi.org/10.2118/107485-pa>
- 701 Giani, G., Orsatti, S., Peter, C., Rocca, V., 2018. A coupled fluid flow-geomechanical approach for
702 subsidence numerical simulation. *Energies* 11. <https://doi.org/10.3390/en11071804>
- 703 Green, A.E., Naghdi, P.M., 1970. The Flow of Fluid through an Elastic Solid. *Acta Mech.* 9, 329–340.
704 <https://doi.org/10.1007/BF01179830>
- 705 Guy, N., Enchéry, G., Renard, G., 2012. Numerical Modeling of Thermal EOR: Comprehensive Coupling of
706 an AMR-Based Model of Thermal Fluid Flow and Geomechanics. *Oil Gas Sci. Technol.* 67, 1019–
707 1027. <https://doi.org/10.2516/ogst/2012052>

- 708 Hatzor, Y.H., 2008. Fundamentals of Discrete Element Methods for Rock Engineering: Theory and
709 Applications. *Int. J. Rock Mech. Min. Sci.* 45, 1536–1537.
710 <https://doi.org/https://doi.org/10.1016/j.ijrmms.2008.04.003>
- 711 Helmig, R., Flemisch, B., Wolff, M., Ebigbo, A., Class, H., 2013. Model coupling for multiphase flow in
712 porous media. *Adv. Water Resour.* 51, 52–66. <https://doi.org/10.1016/j.advwatres.2012.07.003>
- 713 Honarpour, M., Koederitz, L., Harvey, A.H., 1986. Relative permeability of petroleum reservoirs, First. ed,
714 Relative Permeability of Petroleum Reservoirs. CRC Press, New York.
715 <https://doi.org/10.1201/9781351076326>
- 716 Huang, N., Jiang, Y., Liu, R., Li, B., Sugimoto, S., 2019. A novel three-dimensional discrete fracture
717 network model for investigating the role of aperture heterogeneity on fluid flow through fractured
718 rock masses. *Int. J. Rock Mech. Min. Sci.* 116, 25–37. <https://doi.org/10.1016/j.ijrmms.2019.03.014>
- 719 Jalali, M.R., Dusseault, M.B., 2012. Coupling Geomechanics and Transport in Naturally Fractured
720 Reservoirs. *Int. J. Min. Geo-Eng.* 46, 105–131.
- 721 Jerauld, G.R., Salter, S.J., 1990. The Effect of Pore-Structure on Hysteresis in Relative Permeability and
722 Capillary Pressure: Pore-Level Modeling. *Transp. Porous Media* 5, 103–151.
- 723 Jiang, J., Yang, J., 2018. Coupled fluid flow and geomechanics modeling of stress-sensitive production
724 behavior in fractured shale gas reservoirs. *Int. J. Rock Mech. Min. Sci.* 101, 1–12.
725 <https://doi.org/10.1016/j.ijrmms.2017.11.003>
- 726 Jin, M., Somerville, J., Smart, B.G.D., 2000. Coupled Reservoir Simulation Applied to the Management of
727 Production Induced Stress-Sensitivity, in: International Oil and Gas Conference and Exhibition in
728 China. Society of Petroleum Engineers, Beijing, China, pp. 997–1008.
729 <https://doi.org/10.2523/64790-ms>
- 730 Jing, L., 2003. A review of techniques, advances and outstanding issues in numerical modelling for rock
731 mechanics and rock engineering. *Int. J. Rock Mech. Min. Sci.* 40, 283–353.
732 [https://doi.org/10.1016/S1365-1609\(03\)00013-3](https://doi.org/10.1016/S1365-1609(03)00013-3)
- 733 Jing, L., Hudson, J.A., 2002. Numerical methods in rock mechanics. *Int. J. Rock Mech. Min. Sci.* 39, 409–
734 427. [https://doi.org/10.1016/S1365-1609\(02\)00065-5](https://doi.org/10.1016/S1365-1609(02)00065-5)
- 735 Kabele, P., Yamaguchi, E., Horii, H., 1999. FEM-BEM superposition method for fracture analysis of quasi-
736 brittle structures. *Int. J. of Fracture* 100, 249–274.
- 737 Kalinina, E.A., Klise, K.A., McKenna, S.A., Hadgu, T., Lowry, T.S., 2014. Applications of fractured
738 continuum model to enhanced geothermal system heat extraction problems. *Springerplus* 3, 1–13.
739 <https://doi.org/10.1186/2193-1801-3-110>
- 740 Karimi-Fard, M., Durlofsky, L.J., 2016. A general gridding, discretization, and coarsening methodology for
741 modeling flow in porous formations with discrete geological features. *Adv. Water Resour.* 96, 354–
742 372. <https://doi.org/10.1016/j.advwatres.2016.07.019>
- 743 Karimi-Fard, M., Durlofsky, L.J., Aziz, K., 2004. An efficient discrete-fracture model applicable for general-
744 purpose reservoir simulators, in: SPE Reservoir Simulation Symposium. Society of Petroleum
745 Engineers, Houston, Texas, pp. 227–236. <https://doi.org/10.2118/88812-PA>
- 746 Karimi-Fard, M., Durlofsky, L.J., Aziz, K., 2003. An Efficient Discrete Fracture Model Applicable for

747 General Purpose Reservoir Simulators 1–11. <https://doi.org/10.2118/79699-ms>

748 Karimi-Fard, M., Firoozabadi, A., 2003. Numerical simulation of water injection in fractured media using
749 the discrete-fracture model and the Galerkin method. *SPE Reserv. Eval. Eng.* 6, 117–126.
750 <https://doi.org/10.2118/83633-PA>

751 Karimi-Fard, M., Firoozabadi, A., 2001. Numerical Simulation of Water Injection in 2D Fractured Media
752 Using Discrete-Fracture Model, in: *SPE Annual Technical Conference and Exhibition*, 30 September-
753 3 October. Society of Petroleum Engineers, New Orleans, Louisiana. <https://doi.org/SPE-71615-MS>

754 Kazemi, H., Merrill, L.S., 1979. Numerical Simulation of Water Imbibition in Fractured Cores. *Soc. Pet.*
755 *Eng. J.* 19, 175–182. <https://doi.org/10.2118/6895-pa>

756 Keilegavlen, E., Fumagalli, A., Berge, R., Stefansson, I., Berre, I., 2017. PorePy: An Open-Source
757 Simulation Tool for Flow and Transport in Deformable Fractured Rocks.

758 Khalili, N., 2008. Two-phase fluid flow through fractured porous media with deformable matrix. *Water*
759 *Resour. Res.* <https://doi.org/10.1029/2007WR006555>

760 Kim, J., 2010. Sequential methods for coupled geomechanics and multiphase flow. Stanford University.

761 Kim, J., Tchelepi, H.A., Juanes, R., 2013. Rigorous coupling of geomechanics and multiphase flow with
762 strong capillarity. *SPE J.* 18, 1123–1139. <https://doi.org/10.2118/141268-PA>

763 Kim, J., Yang, D., Moridis, G.J., Rutqvist, J., 2012. Numerical studies on two-way coupled fluid flow and
764 geomechanics in hydrate deposits. *SPE J.* 1. <https://doi.org/SPE-141304-PA>

765 Klausen, R.A., Russell, T.F., 2004. Relationships among some locally conservative discretization methods
766 which handle discontinuous coefficients. *Comput. Geosci.* 8, 341–377.
767 <https://doi.org/10.1007/s10596-005-1815-9>

768 Knight, E.E., Rougier, E., Lei, Z., Euser, B., Chau, V., Boyce, S.H., Gao, K., Okubo, K., Froment, M., 2020.
769 HOSS : an implementation of the combined finite - discrete element method. *Comput. Part. Mech.*
770 7, 765–787. <https://doi.org/10.1007/s40571-020-00349-y>

771 Kumar, A., Camilleri, D., Brewer, M., 2016. Comparative analysis of dual continuum and discrete fracture
772 simulation approaches to model fluid flow in naturally fractured, low-permeability reservoirs, in:
773 *SPE Low Perm Symposium*. Society of Petroleum Engineers, Denver, Colorado, USA.
774 <https://doi.org/10.2118/180221-ms>

775 Lavrov, A., 2017. Coupling in hydraulic fracturing simulation, *Porous Rock Fracture Mechanics: With*
776 *Application to Hydraulic Fracturing, Drilling and Structural Engineering*. Elsevier Ltd.
777 <https://doi.org/10.1016/B978-0-08-100781-5.00003-8>

778 Lee, S., Schechter, D.S., 2015. Iteratively coupled fluid flow and geomechanics simulation using
779 estimated equivalent Permeability and porosity by fractal and statistical methods, in: *SPE Annual*
780 *Technical Conference and Exhibition*. <https://doi.org/10.2118/175113-ms>

781 Lee, S.H., Lough, M.F., Jensen, C.L., 2001. Hierarchical modeling of flow in naturally fractured formations
782 with multiple length scales. *Water Resour. Res.* 37, 443–455. <https://doi.org/10.1029/2000WR900340>;
783 <http://dx.doi.org/10.1029/2000WR900340>

784 Lei, G., Liao, Q., Zhang, D., 2019. A new analytical model for flow in acidized fractured-vuggy porous
785 media. *Sci. Rep.* 9, 1–12. <https://doi.org/10.1038/s41598-019-44802-2>

- 786 Lei, Q., Latham, J.P., Tsang, C.F., 2017. The use of discrete fracture networks for modelling coupled
787 geomechanical and hydrological behaviour of fractured rocks. *Comput. Geotech.* 85, 151–176.
788 <https://doi.org/10.1016/j.compgeo.2016.12.024>
- 789 Li, L., Lee, S.H., 2008. Efficient field-scale simulation of black oil in a naturally fractured reservoir through
790 discrete fracture networks and homogenized media. *SPE Reserv. Eval. Eng.* 11, 750–758.
791 <https://doi.org/10.2118/103901-pa>
- 792 Li, L., Shi, A., Wang, X., 2019. A new method for calculating the exchange flux in discrete fracture model
793 for two-phase flow in fractured porous media, in: *IOP Conference Series: Earth and Environmental*
794 *Science*. IOP Science, Dalian, China. <https://doi.org/10.1088/1755-1315/384/1/012087>
- 795 Lipnikov, K., Manzini, G., Svyatskiy, D., 2011. Analysis of the monotonicity conditions in the mimetic
796 finite difference method for elliptic problems. *J. Comput. Phys.* 230, 2620–2642.
797 <https://doi.org/10.1016/j.jcp.2010.12.039>
- 798 Lisjak, A., Grasselli, G., 2014. A review of discrete modeling techniques for fracturing processes in
799 discontinuous rock masses. *J. Rock Mech. Geotech. Eng.* 6, 301–314.
800 <https://doi.org/10.1016/j.jrmge.2013.12.007>
- 801 Lisjak, A., Grasselli, G., 2014. A review of discrete modeling techniques for fracturing processes in
802 discontinuous rock masses. *J. Rock Mech. Geotech. Eng.* 6, 301–314.
803 <https://doi.org/10.1016/j.jrmge.2013.12.007>
- 804 Liu, Z., 2018. *Multiphysics in Porous Materials*, *Multiphysics in Porous Materials*. Springer, Cham, Cham,
805 Switzerland. https://doi.org/10.1007/978-3-319-93028-2_4
- 806 Longuemare, P., Mainguy, M., Lemonnier, P., Onaisi, A., Gérard, C., Koutsabeloulis, N., 2002.
807 *Geomechanics in reservoir simulation: Overview of coupling methods and field case study*. *Oil Gas*
808 *Sci. Technol.* 57, 471–483. <https://doi.org/10.2516/ogst:2002031>
- 809 Majorana, C.E., Salomoni, V.A., Mazzucco, G., Pomaro, B., Xotta, G., 2015. *Mechanical Modelling of*
810 *Concrete and Concrete Structures*. *Comput. Technol. Rev.* 11, 1–29.
811 <https://doi.org/10.4203/ctr.11.1>
- 812 Manouchehrian, A., Marji, M.F., Mohebbi, M., 2012. Comparison of indirect boundary element and
813 finite element methods A case study: Shiraz-Esfahan railway tunnel in Iran. *Front. Archit. Civ. Eng.*
814 *China* 6, 385–392. <https://doi.org/10.1007/s11709-012-0173-7>
- 815 Marcondes, F., Sepehrnoori, K., 2010. An element-based finite-volume method approach for
816 heterogeneous and anisotropic compositional reservoir simulation. *J. Pet. Sci. Eng.* 73, 99–106.
817 <https://doi.org/10.1016/j.petrol.2010.05.011>
- 818 Martin, A., Zhang, H., Tagavi, K.A., 2017. An introduction to the derivation of surface balance equations
819 without the excruciating pain. *Int. J. Heat Mass Transf.* 115, 992–999.
820 <https://doi.org/10.1016/j.ijheatmasstransfer.2017.07.078>
- 821 McCartney, J.S., Sánchez, M., Tomac, I., 2016. *Energy geotechnics: Advances in subsurface energy*
822 *recovery, storage, exchange, and waste management*. *Comput. Geotech.* 75, 244–256.
823 <https://doi.org/10.1016/j.compgeo.2016.01.002>
- 824 McClure, M.W., Horne, R.N., 2013. *Discrete Fracture Network Modeling of Hydraulic Stimulation*, 1st ed.
825 Springer International Publishing. <https://doi.org/10.1007/978-3-319-00383-2>

- 826 Mesquita, E., Pavanello, R., 2005. Numerical methods for the dynamics of unbounded domains. *Comput.*
827 *Appl. Math.* 24, 1–26. <https://doi.org/10.1590/S0101-82052005000100001>
- 828 Mikelić, A., Wang, B., Wheeler, M.F., 2014. Numerical convergence study of iterative coupling for
829 coupled flow and geomechanics. *Comput. Geosci.* 18, 325–341. [https://doi.org/10.1007/s10596-](https://doi.org/10.1007/s10596-013-9393-8)
830 013-9393-8
- 831 Minkoff, S.E., Stone, C.M., Bryant, S., Peszynska, M., Wheeler, M.F., 2003. Coupled fluid flow and
832 geomechanical deformation modeling. *J. Pet. Sci. Eng.* 38, 37–56. [https://doi.org/10.1016/S0920-](https://doi.org/10.1016/S0920-4105(03)00021-4)
833 4105(03)00021-4
- 834 Mohiuddin, M.A., Korvin, G., Abdulraheem, A., Awal, M.R., Khan, K., Khan, M.S., Hassan, H.M., 2000.
835 Stress-Dependent Porosity and Permeability of a Suite of Samples From Saudi Arabian Sandstone
836 and Limestone Reservoirs, in: *International Symposium, Society of Core Analysts. Society of Core*
837 *Analysts, Abu Dhabi*, p. 33.
- 838 Moinfar, A., Narr, W., Hui, M.H., Mallison, B., Lee, S.H., 2011. Comparison of Discrete-Fracture and Dual-
839 Permeability Models for Multiphase Flow in Naturally Fractured Reservoirs, in: *SPE Reservoir*
840 *Simulation Symposium. Society of Petroleum Engineers, Woodlands, Texas, USA*, pp. 84–85.
841 <https://doi.org/SPE-142295-MS>
- 842 Moinfar, A., Varavei, A., Sepehrnoori, K., Johns, R.T., 2014. Development of an Efficient Embedded
843 Discrete Fracture Model for 3D Compositional Reservoir Simulation in Fractured Reservoirs. *SPE J.*
844 19, 289–303. <https://doi.org/10.2118/154246-PA>
- 845 Monteagudo, J.E.P., Firoozabadi, A., 2004. Control-volume method for numerical simulation of two-
846 phase immiscible flow in two- and three-dimensional discrete-fractured media. *Water Resour. Res.*
847 40, 1–20. <https://doi.org/10.1029/2003WR002996>
- 848 Muggerridge, A., Cockin, A., Webb, K., Frampton, H., Collins, I., Moulds, T., Salino, P., 2014. Recovery
849 rates, enhanced oil recovery and technological limits. *Philos. Trans. R. Soc. A Math. Phys. Eng. Sci.*
850 372. <https://doi.org/10.1098/rsta.2012.0320>
- 851 Munjiza, A., 2004. *The Combined Finite-Discrete Element Method*. John Wiley & Sons Ltd, Chichester,
852 West Sussex, England.
- 853 Nick, H.M., 2010. *Towards large-scale modelling of fluid flow in fractured porous media*. Imperial College
854 London.
- 855 Nikolić, M., Roje-Bonacci, T., Ibrahimbegović, A., 2016. OVERVIEW OF THE NUMERICAL METHODS FOR
856 THE MODELLING OF ROCK MECHANICS PROBLEMS. *Teh. Vjesn.* 23, 627–637.
857 <https://doi.org/10.17559/TV-20140521084228>
- 858 Noorishad, J., Mehran, M., 1982. An upstream finite element method for solution of transient transport
859 equation in fractured porous media. *Water Resour. Res.* 18, 588–596.
860 <https://doi.org/10.1029/WR018i003p00588>
- 861 Nordahl, K., Ringrose, P.S., 2008. Identifying the representative elementary volume for permeability in
862 heterolithic deposits using numerical rock models. *Math. Geosci.* 40, 753–771.
863 <https://doi.org/10.1007/s11004-008-9182-4>
- 864 Nordbotten, J.M., Boon, W.M., Fumagalli, A., Keilegavlen, E., 2019. Unified approach to discretization of
865 flow in fractured porous media. *Comput. Geosci.* 23, 225–237. <https://doi.org/10.1007/s10596->

866 018-9778-9

867 Nur, A., Simmons, G., 1969. Stress-Induced Velocity Anisotropy in Rock. an Experimental Study. J.
868 Geophys. Res. 74, 6667–6674. <https://doi.org/10.1029/jb074i027p06667>

869 Oliver, J., Huespe, A.E., Sánchez, P.J., 2006. A comparative study on finite elements for capturing strong
870 discontinuities: E-FEM vs X-FEM. Comput. Methods Appl. Mech. Eng. 195, 4732–4752.
871 <https://doi.org/10.1016/j.cma.2005.09.020>

872 Osorio, J.G., Chen, H., 1999. Numerical Simulation of the Impact of Flow-Induced Geomechanical
873 Response on the Productivity of Stress-Sensitive Reservoirs SPE 51929. Soc. Pet. Eng.

874 Pan, F., Sepehrnoori, K., Chin, L.Y., 2009. A New Solution Procedure for a Fully Coupled Geomechanics
875 and Compositional Reservoir Simulator, in: SPE Reservoir Simulation Symposium. Society of
876 Petroleum Engineers, The Woodlands, Texas, pp. 720–735. <https://doi.org/10.2118/119029-ms>

877 Pan, F., Sepehrnoori, K., Chin, L.Y., 2007. Development of a coupled geomechanics model for a parallel
878 compositional reservoir simulator, in: Proceedings - SPE Annual Technical Conference and
879 Exhibition. Society of Petroleum Engineers, Anaheim, California, U.S.A., pp. 1294–1302.
880 <https://doi.org/10.2523/109867-ms>

881 Pang, G., Chen, W., Sze, K.Y., 2016. A comparative study of finite element and finite difference methods
882 for two-dimensional space-fractional advection-dispersion equation. Adv. Appl. Math. Mech. 8,
883 166–186. <https://doi.org/10.4208/aamm.2014.m693>

884 Pettersen, Ø., 2010. Compaction, permeability, and fluid flow in brent-type reservoirs under depletion
885 and pressure blowdown. Open Pet. Eng. J. 3, 1–13.
886 <https://doi.org/10.2174/1874834101003010001>

887 Potyondy, D.O., Cundall, P.A., 2004. A bonded-particle model for rock. Int. J. Rock Mech. Min. Sci. 41,
888 1329–1364. <https://doi.org/10.1016/j.ijrmms.2004.09.011>

889 Pratt, W.E., Johnson, D.W., 1926. LOCAL SUBSIDENCE OF THE GOOSE CREEK OIL FIELD. J. Geol. 34, 577–
890 590. <https://doi.org/10.1086/623352>

891 Profito, F.J., Giacomini, M., Zachariadis, D.C., Dini, D., 2015. A General Finite Volume Method for the
892 Solution of the Reynolds Lubrication Equation with a Mass-Conserving Cavitation Model. Tribol.
893 Lett. 60, 1–21. <https://doi.org/10.1007/s11249-015-0588-0>

894 Pyrak-Nolte, L.J., Nolte, D.D., Chen, D., Giordano, N.J., 2008. Relating capillary pressure to interfacial
895 areas. Water Resour. Res. 44, 1–14. <https://doi.org/10.1029/2007WR006434>

896 Rao, X., Cheng, L., Cao, R., Jia, P., Dong, P., Du, X., 2019. A modified embedded discrete fracture model
897 to improve the simulation accuracy during early-time production of multi-stage fractured
898 horizontal well, in: Society of Petroleum Engineers - SPE/IATMI Asia Pacific Oil and Gas Conference
899 and Exhibition 2019, APOG 2019. Bali, Indonesia. <https://doi.org/10.2118/196263-ms>

900 Ren, G., Jiang, J., Younis, R.M., 2018. A Model for coupled geomechanics and multiphase flow in
901 fractured porous media using embedded meshes. Adv. Water Resour. 122, 113–130.
902 <https://doi.org/10.1016/j.advwatres.2018.09.017>

903 Rocca, V., 2009. Development of a Fully Coupled Approach for Evaluation of Wellbore Stability in
904 Hydrocarbon Reservoirs. Am. J. Environ. Sci. 5, 781–790.

905 <https://doi.org/10.3844/ajessp.2009.781.790>

906 Royer, P., Auriault, J.L., Lewandowska, J., Serres, C., 2002. Continuum modelling of contaminant
 907 transport in fractured porous media. *Transp. Porous Media* 49, 333–359.
 908 <https://doi.org/10.1023/A:1016272700063>

909 Rutqvist, J., Stephansson, O., 2003. The role of hydrochemical coupling in fractured rock engineering.
 910 *Hydrogeol. J.* 11, 7–40. <https://doi.org/10.1007/s10040-002-0241-5>

911 Sabti, M., Alizadeh, A.H., Piri, M., 2016. Three-phase flow in fractured porous media: Experimental
 912 investigation of matrix-fracture interactions, in: *SPE Annual Technical Conference and Exhibition*.
 913 Society of Petroleum Engineers, Dubai, UAE. <https://doi.org/10.2118/181891-ms>

914 Saikia, K., Ikuku, C.E., Sarkar, B.C., 2018. An integrated approach to discretized 3D modeling of
 915 geomechanical properties for unconventional mature field appraisal in the western Canadian
 916 sedimentary basin. *J. Pet. Explor. Prod. Technol.* 8, 417–429. <https://doi.org/10.1007/s13202-017-0406-3>

917

918 Sanaee, R., Oluyemi, G.F., Hossain, M., Oyenehin, M.B., 2013. Stress effects on flow partitioning in
 919 fractured reservoirs: Equivalent porous media versus poro-elasticity coupled modeling, in: 447th
 920 U.S. Rock Mechanics/Geomechanics Symposium, 23-26 June 2013. American Rock Mechanics
 921 Association, San Francisco, California, pp. 2329–2337. <https://doi.org/ARMA-2013-442>

922 Sanaee, R., Oluyemi, G.F., Hossain, M., Oyenehin, M.B., 2012. Fracture-Matrix Flow Partitioning and
 923 Cross Flow : Numerical Modeling of Laboratory Fractured Core Flood, in: *COMSOL Conference*, 10 –
 924 12 October 2012. Milan. <https://doi.org/10.1016/j.jallcom.2009.01.091>

925 Sangnimnuan, A., Li, J., Wu, K., 2018. Development of Efficiently Coupled Fluid-Flow/Geomechanics
 926 Model To Predict Stress Evolution in Unconventional Reservoirs With Complex-Fracture Geometry.
 927 *SPE J.* 23, 640–660. <https://doi.org/10.2118/189452-pa>

928 Settari, A., Mourits, F.M., 1998. A Coupled Reservoir and Geomechanical Simulation System. *SPE J.*
 929 <https://doi.org/10.2118/50939-PA>

930 Settari, A., Walters, D.A., 2001. Advances in Coupled Geomechanical and Reservoir Modeling With
 931 Applications to Reservoir Compaction. *SPE J.* 6. <https://doi.org/SPE-74142-PA>

932 Shi, G. -h, Goodman, R.E., 1989. Generalization of two-dimensional discontinuous deformation analysis
 933 for forward modelling. *Int. J. Numer. Anal. Methods Geomech.* 13, 359–380.
 934 <https://doi.org/10.1002/nag.1610130403>

935 Shi, G. -H, Goodman, R.E., 1985. Two dimensional discontinuous deformation analysis. *Int. J. Numer.*
 936 *Anal. Methods Geomech.* 9, 541–556. <https://doi.org/10.1002/nag.1610090604>

937 Shojaei, A., Galvanetto, U., Rabczuk, T., Jenabi, A., Zaccariotto, M., 2019. A generalized finite difference
 938 method based on the Peridynamic differential operator for the solution of problems in bounded
 939 and unbounded domains. *Comput. Methods Appl. Mech. Eng.* 343, 100–126.
 940 <https://doi.org/10.1016/j.cma.2018.08.033>

941 Soares, E.J., Thompson, R.L., Niero, D.C., 2015. Immiscible liquid-liquid pressure-driven flow in capillary
 942 tubes: Experimental results and numerical comparison. *Phys. Fluids* 27.
 943 <https://doi.org/10.1063/1.4928912>

- 944 Stefansson, I., Berre, I., Keilegavlen, E., 2018. Finite-Volume Discretisations for Flow in Fractured Porous
945 Media. *Transp. Porous Media* 124, 439–462. <https://doi.org/10.1007/s11242-018-1077-3>
- 946 Stone, T., Bowen, G., Papanastasiou, P., Fuller, J., 2000. Fully coupled geomechanics in a commercial
947 reservoir simulator, in: SPE European Petroleum Conference, 24-25 October. Society of Petroleum
948 Engineers, Paris, France, pp. 45–52. <https://doi.org/10.2523/65107-ms>
- 949 Tavakkoli, M., Mohammadsadeghi, M., Shaheabadi, A., Khajoei, S., Malakooti, R., Beidokhti, M.S., 2009.
950 Deterministic versus stochastic Discrete Fracture Network (DFN) modeling, application in a
951 heterogeneous naturally fractured reservoir, in: Kuwait International Petroleum Conference and
952 Exhibition, 14-16 December. Society of Petroleum Engineers, Kuwait City, Kuwait, pp. 227–249.
953 <https://doi.org/10.2118/127086-ms>
- 954 Terzaghi, K., Peck, R.B., Mesri, G., 1996. *Soil Mechanics in Engineering Practice*, 3rd ed. John Wiley &
955 Sons, Inc., New York City, New York.
- 956 Tham, L.G., Yang, T.H., Tang, C.A., 2004. Progressive failure of jointed rocks. *Int. J. Rock Mech. Min. Sci.*
957 41, 389. <https://doi.org/10.1016/j.ijrmms.2003.12.048>
- 958 Tran, D., Settari, A., Nghiem, L., 2004. New iterative coupling between a reservoir simulator and a
959 geomechanics module. *SPE J.* 9, 362–369. <https://doi.org/10.2118/88989-PA>
- 960 Unsal, E., Matthäi, S.K., Blunt, M.J., 2010. Simulation of multiphase flow in fractured reservoirs using a
961 fracture-only model with transfer functions. *Comput. Geosci.* 14, 527–538.
962 <https://doi.org/10.1007/s10596-009-9168-4>
- 963 Wang, K., Peng, X., Du, Z., Haghghi, M., You, Z., 2016. SPE-182260-MS An Improved Grid Generation
964 Approach for Discrete Fracture Network Modelling Using Line Fracture Concept for Two-Phase
965 Flow Simulation.
- 966 Wang, X., 2020. *Automotive Tire Noise and Vibrations: Analysis, Measurement and Simulation.*
967 Butterworth-Heinemann, Melbourne, VIC, Australia.
968 <https://doi.org/https://doi.org/10.1016/C2018-0-02431-7>
- 969 Warren, J.E., Root, P.J., 1963. The Behavior of Naturally Fractured Reservoirs. *Soc. Pet. Eng. J.* 3, 245–
970 255. <https://doi.org/10.2118/426-pa>
- 971 Weishaupt, K., Joekar-Niasar, V., Helmig, R., 2019. An efficient coupling of free flow and porous media
972 flow using the pore-network modeling approach. *J. Comput. Phys.* X 1.
973 <https://doi.org/10.1016/j.jcpx.2019.100011>
- 974 Wheeler, M.F., Yotov, I., 2006. A Multipoint Flux Mixed Finite Element Method. *SIAM J. Numer. Anal.* 44,
975 2082–2106.
- 976 Wu, Y.-S., 2016. *Multiphase Flow in Fractured Porous Media.* Gulf Professional Publishing, Oxford, UK.
977 <https://doi.org/10.1016/b978-0-12-803848-2.00009-x>
- 978 Wu, Yu Shu., Liu, H.H., Bodvarsson, G.S., 2004. A triple-continuum approach for modeling flow and
979 transport processes in fractured rock. *J. Contam. Hydrol.* 73, 145–179.
980 <https://doi.org/10.1016/j.jconhyd.2004.01.002>
- 981 Wu, Yu Shu, Pan, L., Pruess, K., 2004. A physically based approach for modeling multiphase fracture-
982 matrix interaction in fractured porous media. *Adv. Water Resour.* 27, 875–887.

- 983 <https://doi.org/10.1016/j.advwatres.2004.07.002>
- 984 Wu, Y.S., Qin, G., 2009. A generalized numerical approach for modeling multiphase flow and transport in
985 fractured porous media. *Commun. Comput. Phys.* 6, 85–108.
986 <https://doi.org/10.4208/cicp.2009.v6.p85>
- 987 Wu, Y.S., Qin, G., Ewing, R.E., Efendiev, Y., Kang, Z., Ren, Y., 2006. A multiple-continuum approach for
988 modeling multiphase flow in naturally fractured vuggy petroleum reservoirs, in: *International Oil &*
989 *Gas Conference and Exhibition in China*, 5-7 December. Society of Petroleum Engineers, Beijing,
990 China, pp. 739–750. <https://doi.org/10.2523/104173-ms>
- 991 Xiong, X., Li, B., Jiang, Y., Koyama, T., Zhang, C., 2011. Experimental and numerical study of the
992 geometrical and hydraulic characteristics of a single rock fracture during shear. *Int. J. Rock Mech.*
993 *Min. Sci.* 48, 1292–1302. <https://doi.org/10.1016/j.ijrmmms.2011.09.009>
- 994 Xue, L.L., Chen, S.H., Shahrour, I., 2014. Algorithm of coupled normal stress and fluid flow in fractured
995 rock mass by the composite element method. *Rock Mech. Rock Eng.* 47, 1711–1725.
996 <https://doi.org/10.1007/s00603-013-0500-x>
- 997 Yang, D., Moridis, G.J., Blasingame, T.A., 2014. A fully coupled multiphase flow and geomechanics solver
998 for highly heterogeneous porous media. *J. Comput. Appl. Math.* 270, 417–432.
999 <https://doi.org/10.1016/j.cam.2013.12.029>
- 1000 Yang, X., An, W., Li, W., Zhang, S., 2020. Implementation of a Local Time Stepping Algorithm and Its
1001 Acceleration Effect on Two-Dimensional Hydrodynamic Models. *Water*.
1002 <https://doi.org/10.3390/w12041148>
- 1003 Yang, X., Yan, J., Shiming, W., Yayun, Z., Jianhua, X., Hua, Z., 2018. Characterization of multi-scale
1004 discrete-fracture/matrix interactions in naturally fractured reservoirs using mud loss data, in: *2nd*
1005 *International Discrete Fracture Network Engineering Conference*, 20-22 June. American Rock
1006 Mechanics Association, Seattle, Washington, USA. <https://doi.org/ARMA-DFNE-18-0294>
- 1007 Yang, Z.D., Wang, Y., Zhang, X.Y., Qin, M., Su, S.W., Yao, Z.H., Liu, L., 2020. Numerical Simulation of a
1008 Horizontal Well With Multi-Stage Oval Hydraulic Fractures in Tight Oil Reservoir Based on an
1009 Embedded Discrete Fracture Model. *Front. Energy Res.* 8, 1–12.
1010 <https://doi.org/10.3389/fenrg.2020.601107>
- 1011 Yao, C., He, C., Yang, J., Jiang, Q., Huang, J., Zhou, C., 2019. A novel numerical model for fluid flow in 3D
1012 fractured porous media based on an equivalent matrix-fracture network. *Geofluids* 2019, 13.
1013 <https://doi.org/10.1155/2019/9736729>
- 1014 Youssef, A.A.A., Alnuaim, S., 2017. IPR of Triple Continuum Reservoirs, Analytical Approach, in: *SSPE*
1015 *Kingdom of Saudi Arabia Annual Technical Symposium and Exhibition*, 24-27 April. Society of
1016 Petroleum Engineers, Dammam, Saudi Arabia, pp. 2294–2304. <https://doi.org/10.2118/187973-ms>
- 1017 Zareidarmiyani, A., Salarirad, H., Vilarrasa, V., De Simone, S., Olivella, S., 2018. Geomechanical response
1018 of fractured reservoirs. *Fluids* 3, 1–17. <https://doi.org/10.3390/fluids3040070>
- 1019 Zhang, N., Abushaikha, A.S., 2019. Fully implicit reservoir simulation using mimetic finite difference
1020 method in fractured carbonate reservoirs. *Soc. Pet. Eng. - SPE Reserv. Characterisation Simul. Conf.*
1021 *Exhib. 2019, RCSC 2019*. <https://doi.org/10.2118/196711-ms>
- 1022 Zhang, Q., Yao, J., Huang, Z., Li, Y., Zhang, K., 2019. Hybrid multiscale method for numerical modeling of

- 1023 coupled flow and geomechanics. *J. Pet. Sci. Eng.* 176, 943–951.
1024 <https://doi.org/10.1016/j.petrol.2019.02.009>
- 1025 Zhangxin, C., Guanren, H., Yuanle, M., 2006. *Computational Methods for Multiphase Flows in Porous*
1026 *Media*. Society for Industrial and Applied Mathematics, Philadelphia.
- 1027 Zhao, L., Haniao, J., Zhang, S., Hanxu, Y., Fernrui, S., Yan, Q., Lijun, Z., Wenbin, C., Junjian, L., 2018.
1028 Modeling vertical well in field-scale discrete fracture-matrix model using a practical pseudo inner-
1029 boundary model. *J. Pet. Sci. Eng.* 166, 510–530. <https://doi.org/10.1016/j.petrol.2018.02.061>
- 1030 Zhao, M., Zhang, Q., Li, S., Zhao, H., 2017. Investigation on coupled fluid-flow and stress in dual model
1031 rock mass with time-dependent effect and its simulation. *Geosci.* 7, 1–14.
1032 <https://doi.org/10.3390/geosciences7030045>
- 1033 Zhao, N., 2012. *INTEGRATION OF RESERVOIR SIMULATION AND GEOMECHANICS*. The University of Utah.
- 1034 Zoback, M.D., 2007. *Reservoir Geomechanics*, 1st ed, *Reservoir Geomechanics*. Cambridge University
1035 Press, Cambridge. <https://doi.org/10.1017/CBO9780511586477>
- 1036